Available online at www.sciencedirect.com
ScienceDirect
Journal of Computational Physics 221 (2007) 370–394
JOURNAL OF COMPUTATIONAL PHYSICS
www.elsevier.com/locate/jcp

Extrinsic meshfree approximation using asymptotic expansion for interfacial discontinuity of derivative

Do Wan Kim [a,1], Young-Cheol Yoon [b], Wing Kam Liu [b,*], Ted Belytschko [b]

[a] *Department of Applied Mathematics, College of Science and Technology, Hanyang University, Ansan, Kyeonggi-do 426-791, Republic of Korea*
[b] *Department of Mechanical Engineering, Northwestern University, Evanston, IL 60208, USA*

Received 1 November 2004; received in revised form 12 June 2006; accepted 14 June 2006
Available online 17 August 2006

Abstract

A sharp meshfree approximation for derivative discontinuities across arbitrary interfaces is proposed. The interface can be arbitrarily located in a domain in which nodes are distributed uniformly or irregularly. The proposed meshfree approximations consist of two parts, singular and regular. The moving least square meshfree approximation is used together with the local wedge function as basis functions. The approximations for discontinuities are applied in a meshfree point collocation method to obtain solutions of the Poisson problem with a layer delta source on the interface and second order elliptic problems with discontinuous coefficients and/or the singular layer sources along the interface. The numerical calculations show that this method has good performance even on irregular node models.

PACS: 02.70.Jn; 02.60.Cb; 02.60.Jh

Keywords: Arbitrary interface; Extrinsic meshfree approximation; Local wedge function; Meshfree point collocation method; Discontinuous coefficients; Elliptic problem

1. Introduction

In the natural world as well as in the engineering fields, various kinds of discontinuities occur over an interface. They are well known to be difficult to analyze accurately and robustly in numerical computations when the interface is arbitrarily placed on a computational domain. In developing a method to treat such arbitrary discontinuities over interfaces, it is important to construct the approximation with a derivative discontinuity and to design a robust scheme [4,12,13,21,23,25].

* Corresponding author. Tel.: +1 847 491 7094; fax: +1 847 491 3915.
E-mail address: w-liu@northwestern.edu (W.K. Liu).
URL: http://www.tam.northwestern.edu/wkl/liu.html (W.K. Liu).
[1] Visiting Scholar in 2004, Department of Mechanical Engineering, Northwestern University, Evanston, IL 60208, USA.

0021-9991/$ - see front matter
doi:10.1016/j.jcp.2006.06.023

In recent decades, for problems involving discontinuities on a curve in 2-D or a surface in 3-D, the immersed boundary method (IBM) by Peskin [25] and his coworkers has been developed and applied to many biological problems. In this case, the discontinuity on a fluid–solid interface yields the Dirac delta interaction force and IBM provides a means to effectively distribute the concentrated force to the vicinity of the interface. Using a diffuse numerical Dirac delta function in IBM takes advantage of lower cost, while its trade-off is the loss of accuracy. To provide better accuracy in treating discontinuities across the interface, the immersed interface method (IIM) was proposed by LeVeque and Li [13,14]. Additionally, attempts to extensions of IIM have been made for elliptic equations with variable coefficients as seen in [3,26]. For the same purpose of capturing sharp discontinuities, the boundary condition capturing method in [19] that stems from the ghost fluid method (GFM) by Fedkiw et al. [5] has been applied to the variable coefficient Poisson equation with Dirichlet boundary conditions on the irregular interface [6]. A few years ago, the convergence of the GFM for elliptic equations with interfaces was proved in [20] by using a weak formulation.

However, we still need the pseudo-spectral approximation for the interfacial discontinuities to calculate the approximated sharp discontinuous values on both sides of the interface. The finite element approximation can be one candidate in this viewpoint. The immersed finite element method (IFEM) by Liu et al. [15,27] is a method to model the interfacial force on a body induced by the background flow where an Eulerian mesh is used for the flow and Lagrangian mesh for the moving body. In IFEM, both fluid and solid domains are modeled with the finite element method and the continuity between fluid and solid subdomains is enforced via the interpolation of the velocities and the distribution of the interaction forces with the reproducing Kernel particle method (RKPM) delta function [16,17]. In the extended finite element method (XFEM) [24] to analyze the moving discontinuities in function and gradients, the jump function and crack tip singularities are introduced to approximate the discontinuous displacements for a crack. An important theoretical result in finite element methods for the elliptic problems with discontinuous coefficients has been reported by Babuška [1]. According to his early work, sub-optimal convergence rate of the numerical solution in the H^1 norm is of $O(h^{\frac{1}{2}})$ when the interface runs through the interior of elements. This means that no treatment of discontinuity can guarantee optimal convergence. In [8], a discontinuity treatment is developed for the variable coefficient elliptic equation even with non-smooth interfaces and the convergences of various examples were tested numerically. As another example of a pseudo-spectral discontinuity treatment, the discontinuous reproducing kernel element method can be seen in [22].

In this paper, keeping the meshfree point collocation method in mind, we first develop meshfree pseudo-spectral approximations of continuous functions with a finite jump of the normal derivative across the interface (i.e. a weak discontinuity). Next, using these approximations, we use the point collocation schemes to solve elliptic equations with discontinuous coefficients and/or the singular layer sources over an interface.

Based on the exact extraction of the leading singular behavior from the function having the interfacial discontinuities, we apply the approximation to the meshfree point collocation method to obtain the numerical solution of elliptic problems with discontinuous coefficients and/or singular layer sources over an interface. The important issue in this approach is to make a discretization of the interface condition. Our approximations are defined at any point in the problem domain, so that the modeling nodes for the interface can be placed arbitrarily.

On the other hand, since the interface conditions are defined on the interface, the linear interface element approximation is introduced only for the approximation of the unknown jump in the normal derivative. According to the numerical results obtained, the proposed approximation yields a sharp approximation of derivatives of the numerical solution without smearing near the interface. Moreover, it is so robust that the optimal convergence for the extrinsic meshfree derivative of the numerical solution can be maintained independent of the interface discretization for the unknown jump approximation and the jump values of the discontinuous coefficients across the interface in the partial differential equations. Although the numerical experiments were done in 2-D problems, the method proposed in this paper is expected to be directly applicable to 3-D once the interfacial surface is modeled effectively enough to approximate a function on it.

2. Discontinuous meshfree approximation

Let Ω be a bounded domain in $\mathbb{R}^d$ and $\Lambda \equiv \{\mathbf{x}_I \in \overline{\Omega} | I = 1, \ldots, N\}$ be an admissible set of nodes in $\overline{\Omega}$ where d is the space dimension; $\rho_{\mathbf{x}}$ in this paper designates the dilation function which takes the place of the dilation

parameter and depends on the set Λ of nodes: it has to be a continuous and positive function on $\overline{\Omega}$ compatible with the completeness of the basis polynomials up to order m. By the admissible set of nodes in the above, we mean that there exists a dilation function $\rho_{\mathbf{x}}$ such that the moment matrix related to $\rho_{\mathbf{x}}$ is regular. It is proven, in [10], that a set of uniform nodes is an admissible set and the convergence for the meshfree point collocation method without interface occurs. Similarly, some necessary conditions for the admissibility of nodes are reported in [7,15]. A successful approach to calculate such $\rho_{\mathbf{x}}$ for a given admissible node distribution has been proposed in [9].

2.1. Notations and symbols involving interface discontinuities

Throughout the paper, multi-index notations are employed. Let $\alpha = (\alpha_1, \ldots, \alpha_d)$ be the d-tuple of non-negative integers called the multi-index and $\mathbf{x} = (x_1, \ldots, x_d) \in \mathbb{R}^d$ be a d-dimensional real vector. Then the length and the factorial of α are defined by $|\alpha| \equiv \sum_{i=1}^{d} \alpha_i$ and $\alpha! \equiv \alpha_1! \ldots \alpha_d!$, respectively. The αth power of $\mathbf{x}$ and the αth partial derivative operator are defined as follows:

$$\mathbf{x}^{\alpha} \equiv x_1^{\alpha_1} x_2^{\alpha_2} \ldots x_d^{\alpha_d}, \quad D_{\mathbf{x}}^{\alpha} \equiv \partial_{x_1}^{\alpha_1} \partial_{x_2}^{\alpha_2} \ldots \partial_{x_d}^{\alpha_d}. \tag{1}$$

Let Γ designate the interface defined as a bounded $(d-1)$-dimensional smooth manifold (locally diffeomorphic $(d-1)$-dimensional Euclidean space) with or without boundary embedded in Ω. We consider the function space $C_B^{m+1}(\Omega \setminus \Gamma)$ defined by

$$C_B^{m+1}(\Omega \setminus \Gamma) \equiv \{u(\mathbf{x}) \in C^{m+1}(\Omega \setminus \Gamma) | D^{\beta} u \text{ is bounded and uniformly continuous in } \Omega \setminus \Gamma \text{ for all } |\beta| \leqslant m+1\}. \tag{2}$$

The function space of all bounded and uniformly continuous functions in $\overline{\Omega}$ is denoted by $C^0(\overline{\Omega})$. The aim in this section is to describe how to effectively approximate functions in $C_B^{m+1}(\Omega \setminus \Gamma) \cap C^0(\overline{\Omega})$ using the discontinuous meshfree method.

The average and jump of function values at a point $\mathbf{x}$ on the interface Γ are expressed as follows:

$$\mathbf{x}^{\pm} = \lim_{t \to 0^{\pm}} \mathbf{x} + t\mathbf{n}, \tag{3}$$

$$\langle D^{\alpha} u \rangle_{\mathbf{x}} = \frac{1}{2} (D^{\alpha} u|_{\mathbf{x}^+} + D^{\alpha} u|_{\mathbf{x}^-}), \tag{4}$$

$$[D^{\alpha} u]_{\mathbf{x}} = D^{\alpha} u|_{\mathbf{x}^+} - D^{\alpha} u|_{\mathbf{x}^-}, \tag{5}$$

where $\mathbf{n}$ is a unit normal vector to Γ at $\mathbf{x}$. Since the average and jump, $\langle D^{\alpha} u \rangle_{\mathbf{x}}$ and $[D^{\alpha} u]_{\mathbf{x}}$, respectively, can be seen as a function defined on Γ, we often use alternative notations, $\langle D^{\alpha} u \rangle_{\Gamma}$ and $[D^{\alpha} u]_{\Gamma}$, instead.

In our case dealing, it is necessary to calculate the projection mapping and unit normal vector function on a neighborhood of the interface. As illustrated in Fig. 1, for given interface Γ and a neighborhood Ω^{S} of Γ which is to be determined, if $\bar{\mathbf{x}}$ is a point in Ω^{S}, then $\bar{\mathbf{x}}_{\Gamma} \in \Gamma$ and $\mathbf{n}_{\Gamma}(\bar{\mathbf{x}})$ are the projection point of $\bar{\mathbf{x}}$ and the unit normal vector toward $\bar{\mathbf{x}}$, respectively, which are defined as follows:

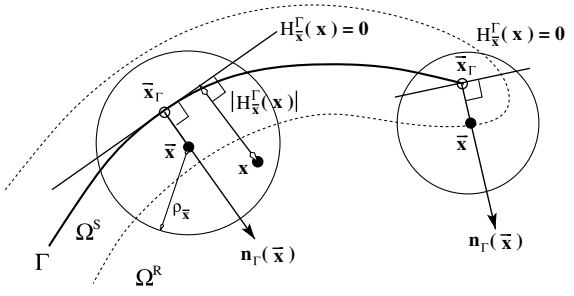

Fig. 1. Illustration of the singular region Ω^{S} and the regular region Ω^{R}, definitions of the maps $\bar{\mathbf{x}}_{\Gamma} \equiv \mathrm{proj}_{\Gamma}(\bar{\mathbf{x}})$ and $\mathbf{n}_{\Gamma}(\bar{\mathbf{x}}) \equiv \frac{\mathbf{x} - \bar{\mathbf{x}}_{\Gamma}}{|\mathbf{x} - \bar{\mathbf{x}}_{\Gamma}|}$ where $H_{\bar{\mathbf{x}}}^{\Gamma}(\mathbf{x}) \equiv \mathbf{n}_{\Gamma}(\bar{\mathbf{x}}) \cdot (\mathbf{x} - \bar{\mathbf{x}}_{\Gamma})$ represents the linear function of $\mathbf{x}$.

$$\bar{\mathbf{x}}_\Gamma \equiv \mathrm{Proj}_\Gamma \bar{\mathbf{x}} : \|\bar{\mathbf{x}}_\Gamma - \bar{\mathbf{x}}\| = \inf_{\mathbf{y}\in\Gamma} \|\mathbf{y} - \bar{\mathbf{x}}\|, \tag{6}$$

$$\mathbf{n}_\Gamma(\bar{\mathbf{x}}) \equiv \frac{\bar{\mathbf{x}} - \bar{\mathbf{x}}_\Gamma}{|\bar{\mathbf{x}} - \bar{\mathbf{x}}_\Gamma|}. \tag{7}$$

In general, the projection map in (6) can have multiple values. Hence, the map $\mathbf{n}_\Gamma(\bullet)$ in (7) may become a multi-valued function as well.

Remark 1. It is worth noting that the map $\mathbf{n}_\Gamma(\bar{\mathbf{x}})$ equals the usual normal vector emanating from the projection point $\bar{\mathbf{x}}_\Gamma$ toward $\bar{\mathbf{x}}$ unless $\bar{\mathbf{x}}_\Gamma$ becomes the end(or boundary) point of Γ. Since manifolds with or without a boundary can be seen as locally $(d-1)$-dimensional Euclidean or half Euclidean spaces, respectively, there exists an open region sufficiently small near the interface on which the mapping (6) can be made well-defined.

The singular region(or neighborhood) of Γ, denoted by the symbol Ω^{S} as seen in Fig. 1, is defined by using a dilation function $\rho_{\mathbf{x}}$ such that

$$\Omega^{\mathrm{S}} \equiv \{\mathbf{x} \in \overline{\Omega} | \mathrm{dist}(\mathbf{x}, \Gamma) < \rho_{\mathbf{x}}\}, \tag{8}$$

where dist($\mathbf{x}$,Γ) denotes the minimum distance between $\mathbf{x}$ and points in Γ. On the other hand, the regular region Ω^{R} in Fig. 1 is defined by the complement of the singular region Ω^{S}, i.e.,

$$\Omega^{\mathrm{R}} \equiv \overline{\Omega} \setminus \Omega^{\mathrm{S}}. \tag{9}$$

In general, finer models can reduce the dilation function values. Consequently, the projection mapping in (6) can be made a well-defined mapping on the singular region Ω^{S} theoretically if the models are fine enough. From this reason, the singular region Ω^{S} will be assumed to be a neighborhood of Γ on which the projection (6) is well-defined.

On the other hand, if the function $u(\mathbf{x}) \in C_B^{m+1}(\Omega \setminus \Gamma) \cap C^0(\overline{\Omega})$ is composed of the singular and regular parts such that

$$u(\mathbf{x}) = u^{\mathrm{S}}(\mathbf{x}) + u^{\mathrm{R}}(\mathbf{x}) \tag{10}$$

for some $u^{\mathrm{R}}(\mathbf{x}) \in C^1(\overline{\Omega})$, then a series of approximations for $u(\mathbf{x})$ are desired to accurately extract the singular part $u_h^{\mathrm{S},[\beta]}$ corresponding to that of $D^\beta u(\mathbf{x})$ such that

$$(\mathscr{D}_h^\beta u)(\mathbf{x}) = u_h^{\mathrm{S},[\beta]}(\mathbf{x}) + u_h^{\mathrm{R},[\beta]}(\mathbf{x}), \quad |\beta| \leqslant 1, \tag{11}$$

where $u_h^{\mathrm{S},[\beta]}(\mathbf{x})$ behaves like $D^\beta u^{\mathrm{S}}(\mathbf{x})$ near the interface at least for each multi-index $|\beta| \leqslant 1$ and $u_h^{\mathrm{R},[\beta]}(\mathbf{x})$'s are continuous. To do so, we have to know the asymptotic behavior of the function $u(\mathbf{x}) \in C_B^{m+1}(\Omega \setminus \Gamma) \cap C^0(\overline{\Omega})$ near the interface and then extract the singularity from $u(\mathbf{x})$.

2.2. Local asymptotic approximation of functions in $C_B^{m+1}(\Omega \setminus \Gamma) \cap C^0(\overline{\Omega})$ near Γ and introduction to local wedge function

Let $B_r(\mathbf{x})$ be the open r-ball in $\mathbb{R}^d$ centered at $\mathbf{x}$. From the definition of Ω^{S}, the local region $B_{\rho_{\bar{\mathbf{x}}}}(\bar{\mathbf{x}})$ for every $\bar{\mathbf{x}} \in \Omega^{\mathrm{S}}$ touches the interface. On such balls, the local asymptotic approximation of $u(\mathbf{x})$ in $C_B^{m+1}(\Omega \setminus \Gamma) \cap C^0(\overline{\Omega})$ is of interest and the effect of the interface discontinuity must be considered in the approximation as well in view of the meshfree approximation of $u(\mathbf{x})$.

The asymptotic expansion for the function $u(\mathbf{x}) \in C_B^{m+1}(\Omega \setminus \Gamma)$ is stated in Lemma 4 in Appendix A together with its proof. According to Lemma 4, if the center of expansion(written as $\mathbf{x}$ in (64)) is replaced with the projection point $\bar{\mathbf{x}}_\Gamma \in \Gamma$ and the space variable $\mathbf{y}$ in (64) is done with the conventional variable $\mathbf{x}$, then an effective local approximation of the function $u(\mathbf{x})$ on $B_{\rho_{\bar{\mathbf{x}}}}(\bar{\mathbf{x}})$ can be obtained as follows:

$$\begin{aligned} u(\mathbf{x}) = {} & \frac{1}{2}\mathrm{sign}((\mathbf{x} - \bar{\mathbf{x}}_\Gamma)\cdot\mathbf{n})[u]_{\bar{\mathbf{x}}_\Gamma} + \frac{1}{2}\ \mathrm{sign}((\mathbf{x} - \bar{\mathbf{x}}_\Gamma)\cdot\mathbf{n})(\mathbf{x} - \bar{\mathbf{x}}_\Gamma)\cdot[\nabla u]_{\bar{\mathbf{x}}_\Gamma} \\ & + \frac{1}{2}\mathrm{sign}((\mathbf{x} - \bar{\mathbf{x}}_\Gamma)\cdot\mathbf{n}) \sum_{2\leqslant|\alpha|\leqslant m} \frac{[D^\alpha u]_{\bar{\mathbf{x}}_\Gamma}}{\alpha!}(\mathbf{x} - \bar{\mathbf{x}}_\Gamma)^\alpha + \sum_{|\alpha|\leqslant m} \frac{\langle D^\alpha u\rangle_{\bar{\mathbf{x}}_\Gamma}}{\alpha!}(\mathbf{x} - \bar{\mathbf{x}}_\Gamma)^\alpha + R_m(\mathbf{x} - \bar{\mathbf{x}}_\Gamma; \bar{\mathbf{x}}_\Gamma) \end{aligned} \tag{12}$$

for all $\mathbf{x} \in B_{\rho_{\bar{\mathbf{x}}}}(\bar{\mathbf{x}})$, where the function sign(•) implies the sign of its argument (•). Moreover, the remainder term is estimated as follows:

$$|R_m(\mathbf{x} - \bar{\mathbf{x}}_\Gamma; \bar{\mathbf{x}}_\Gamma)| \leqslant C\rho_{\bar{\mathbf{x}}}^{m+1} \tag{13}$$

for some constant $C > 0$ depending only on u (see Appendix A).

From now on, we focus on the case where $u \in C_B^{m+1}(\Omega \setminus \Gamma) \cap C^0(\overline{\Omega})$. The first term in (12) must vanish since the function u is assumed continuous across Γ, i.e.,

$$[u]_{\bar{\mathbf{x}}_\Gamma} = 0. \tag{14}$$

If decomposing the second term in (12) into normal and tangential components on Γ, it is simplified as the following:

$$\frac{1}{2}|(\mathbf{x} - \bar{\mathbf{x}}_\Gamma) \cdot \mathbf{n}_\Gamma(\bar{\mathbf{x}})| \left[\frac{\partial u}{\partial n}\right]_{\bar{\mathbf{x}}_\Gamma} \tag{15}$$

since the tangential component vanishes from the continuity on Γ. In (15), the absolute value is only an emphasis as far as $\mathbf{n}_\Gamma(\bullet)$ is employed instead of the usual normal vector $\mathbf{n}$ when $\bar{\mathbf{x}}_\Gamma$ is replaced with x. The local approximation of (12) is useful in separating the singularities up to first order derivatives located at the point $\bar{\mathbf{x}}_\Gamma$. As a consequence, the resultant local approximation has the following form:

$$u(\mathbf{x}) = \underbrace{\frac{1}{2}|(\mathbf{x} - \bar{\mathbf{x}}_\Gamma) \cdot \mathbf{n}_\Gamma(\bar{\mathbf{x}})| \left[\frac{\partial u}{\partial n}\right]_{\bar{\mathbf{x}}_\Gamma}}_{\text{Singular Part}} + \underbrace{u^{\mathrm{R}}(\mathbf{x}, \bar{\mathbf{x}})}_{\text{Regular Part}}, \quad \forall \mathbf{x} \in B_{\rho_{\bar{\mathbf{x}}}}(\bar{\mathbf{x}}), \tag{16}$$

where $u^{\mathrm{R}}(\mathbf{x}, \bar{\mathbf{x}})$ is differentiable at $\bar{\mathbf{x}}$.

The leading term of (16) causes the major singularity of first derivatives at $\bar{\mathbf{x}}$ and its graph looks like a wedge (see Fig. 2 (a)). Thus, we will call it *the local wedge function* and employ the following notation for simplicity:

$$b_\Gamma(\mathbf{x}, \bar{\mathbf{x}}) \equiv |(\mathbf{x} - \bar{\mathbf{x}}_\Gamma) \cdot \mathbf{n}_\Gamma(\bar{\mathbf{x}})|. \tag{17}$$

The derivatives of $b_\Gamma(\mathbf{x}, \bar{\mathbf{x}})$ with respect to the first argument $\mathbf{x}$ are needed for later use and, if $\omega(t) = t$, then we address those as follows:

$$D_{\mathbf{x}}^{\beta} b_\Gamma(\mathbf{x}, \bar{\mathbf{x}}) = \mathbf{n}_\Gamma(\bar{\mathbf{x}})^{\beta} \omega^{(|\beta|)}(b_\Gamma(\mathbf{x}, \bar{\mathbf{x}})), \quad \mathbf{x} \notin \Gamma \tag{18}$$

for any multi-index $\beta, |\beta| \leqslant m$, where $\omega^{(|\beta|)}(\bullet)$ is $|\beta|$-order derivative of the function $\omega(\bullet)$. The limit values of these derivatives are obtained by taking the limit as $\bar{\mathbf{x}}$ approaches $\mathbf{x}$:

$$D_{\mathbf{x}}^{\beta} b_\Gamma(\mathbf{x}, \bar{\mathbf{x}})|_{\bar{\mathbf{x}}=\mathbf{x}} = \mathbf{n}_\Gamma(\mathbf{x})^{\beta} \omega^{(|\beta|)}(|\mathbf{x} - \mathbf{x}_\Gamma|), \quad \mathbf{x} \notin \Gamma. \tag{19}$$

It is worth noting that, unless we assume the continuity of $u(\mathbf{x})$(i.e. a strong discontinuity), two leading singular terms, the first and second terms in (12) should be considered simultaneously. However, in this paper,

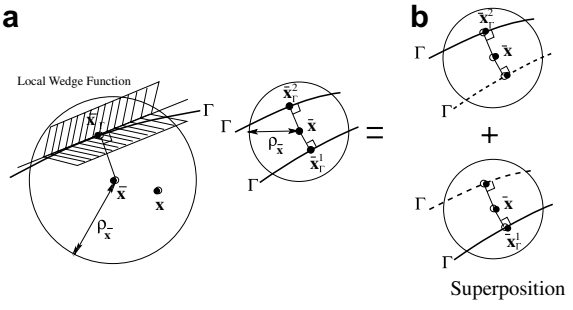

Fig. 2. (a) Local asymptotic expansion region $B_{\rho_{\bar{\mathbf{x}}}}(\bar{\mathbf{x}})$ and local wedge function and (b) superposition is available if the local region $B_{\rho_{\bar{\mathbf{x}}}}(\bar{\mathbf{x}})$ contains disjoint multi-interfaces.

we will not discuss such discontinuities any further since we consider only the derivative discontinuity across the interface.

As shown in Fig. 2 (b), if a finite number of disjoint interfaces run through the local region $B_{\rho_{\bar{\mathbf{x}}}}(\bar{\mathbf{x}})$, then the superposition principle is available, i.e., the sum of multiple local wedge functions for the corresponding projection points can extract the effective discontinuities in $B_{\rho_{\bar{\mathbf{x}}}}(\bar{\mathbf{x}})$. However, in this paper, only one interface is considered in such case for the short description of the method.

The local wedge function used here is similar to the distance function in the finite element formulation given by Belytschko et al. [2]. Our local wedge function is defined locally, so that it is different from the method before. The localization deserves emphasizing in this paper.

2.3. Extrinsic meshfree approximations equipped with the normal derivative jump

Based on the singularity analysis in Section 2.2 for the function with a finite jump in the derivative across the smooth interface, the moving least square (MLS) approximation (see [10,11,18]) for the regular part of $u(\mathbf{x})$ is constructed using the following vector of complete polynomials up to order m

$$\mathbf{P}_m(\mathbf{x},\bar{\mathbf{x}}) = \left[\left(\frac{\mathbf{x}-\bar{\mathbf{x}}}{\rho_{\bar{\mathbf{x}}}}\right)^{\alpha_1},\ldots,\left(\frac{\mathbf{x}-\bar{\mathbf{x}}}{\rho_{\bar{\mathbf{x}}}}\right)^{\alpha_L}\right], \tag{20}$$

where $\alpha_1 = (0,\ldots,0)$, $\alpha_2 = (1,0,,\ldots,0)$, $\alpha_3 = (0,1,0,\ldots,0),\ldots,$ $\alpha_L = (0,\ldots,0,m)$.

Inspired by the local extraction of the jump discontinuity of the normal derivative as in (16), we propose the local MLS approximation of $u(\mathbf{x})$ near $\bar{\mathbf{x}} \in \overline{\Omega}$ as the following:

$$u_{\bar{\mathbf{x}}}(\mathbf{x}) \equiv \underbrace{\frac{1}{2}\left[\frac{\partial u}{\partial n}\right]_{\bar{\mathbf{x}}_\Gamma} \chi_{\Omega^S}(\bar{\mathbf{x}}) b_\Gamma(\mathbf{x},\bar{\mathbf{x}})}_{\text{Singular Part Approximation}} + \underbrace{\mathbf{a}(\bar{\mathbf{x}})\cdot\mathbf{P}_m(\mathbf{x},\bar{\mathbf{x}})}_{\text{Regular Part Approximation}}, \quad \forall \mathbf{x} \in B_{\rho_{\bar{\mathbf{x}}}}(\bar{\mathbf{x}}), \tag{21}$$

where $\chi_{\Omega^S}(\mathbf{x})$ represents the characteristic function of the singular region Ω^S and $\mathbf{a}(\bar{\mathbf{x}})$ is the vector of unknown coefficients which depends on $\bar{\mathbf{x}}$. To determine the best coefficients $\mathbf{a}(\bar{\mathbf{x}})$ of the local approximation (21) in the locally weighted moving least square sense for the given set of nodes Λ, the following locally weighted functional has to be minimized at each $\bar{\mathbf{x}}$

$$J_{\bar{\mathbf{x}}}(\mathbf{a}) \equiv \sum_{\mathbf{x}_I \in \Lambda} |u(\mathbf{x}_I) - u_{\bar{\mathbf{x}}}(\mathbf{x}_I)|^2 W_{\bar{\mathbf{x}}}(\mathbf{x}_I), \tag{22}$$

where $W_{\bar{\mathbf{x}}}(\mathbf{x}) \equiv W\left(\frac{\mathbf{x}-\bar{\mathbf{x}}}{\rho_{\bar{\mathbf{x}}}}\right)$ is defined from the given window function $W(\mathbf{x})$ of the following form (see [10]):

$$W(\mathbf{x}) \equiv \begin{cases} (1-|\mathbf{x}|^{\frac{1}{2}})^2, & \text{for } |\mathbf{x}|<1, \mathbf{x}\in\mathbb{R}^d, \\ 0, & \text{otherwise.} \end{cases} \tag{23}$$

Under these settings for MLS method (see Appendix B) the standard MLS procedure for $u(\mathbf{x}) \in C_B^{m+1}(\Omega\setminus\Gamma) \cap C^0(\overline{\Omega})$ yields a new meshfree approximation such that, for any β, $|\beta| \leqslant m$,

$$\mathscr{D}_h^\beta u(\mathbf{x}) = \underbrace{\frac{1}{2}\left[\frac{\partial u}{\partial n}\right]_{\mathbf{x}_\Gamma} \chi_{\Omega^S}(\mathbf{x}) S_\Gamma^{[\beta]}(\mathbf{x})}_{\text{Singular Part of } \beta\text{th derivative}} + \sum_{\mathbf{x}_I\in\Lambda} u(\mathbf{x}_I)\psi_I^{[\beta]}(\mathbf{x}), \quad \forall \mathbf{x}\in\Omega\setminus\Gamma, \tag{24}$$

where $\psi_I^{[\beta]}(\mathbf{x})$ is the shape function defined by (83) in Appendix B and $S_\Gamma^{[\beta]}(\mathbf{x})$ will be called *the extrinsic βth order singular shape function for Γ* and is defined by

$$S_\Gamma^{[\beta]}(\mathbf{x}) \equiv D_{\mathbf{x}}^\beta b_\Gamma(\mathbf{x},\bar{\mathbf{x}})|_{\bar{\mathbf{x}}=\mathbf{x}} - \sum_{\mathbf{x}_I\in\Lambda} b_\Gamma(\mathbf{x}_I,\mathbf{x})\psi_I^{[\beta]}(\mathbf{x}). \tag{25}$$

We will call these approximations in (24) *the extrinsic meshfree approximations*. The derivation of these approximations is shown in detail in Appendix B for self-containedness.

Remark 2

(1) In the first term of (24), we need to point out that $\left[\frac{\partial u}{\partial n}\right]_{\mathbf{x}_\Gamma}$ is a composite function defined not on Γ but on Ω^{S}, i.e.,

$$\left[\frac{\partial u}{\partial n}\right]_{\mathbf{x}_\Gamma} = \left[\frac{\partial u}{\partial n}\right]_{\Gamma} \circ \mathrm{proj}_\Gamma \mathbf{x} : \Omega^s \to \mathbb{R}. \tag{26}$$

This fact is used in developing the point collocation method.

(2) The computational cost in calculating the shape function $\psi_I^{[\beta]}(\mathbf{x})$ is in doing the inverse of the moment matrix at $\mathbf{x}$. If $L = \frac{(m+d)!}{m!d!}$ and the number of node $\mathbf{x}_I$'s contained in the support of window function at $\mathbf{x}$ is assumed to be $N_{\mathbf{x}}$, then the cost to compute the moment matrix is of order $\mathrm{O}(L^2)$ and the operation count in inversion of the moment matrix for all I is of $\mathrm{O}(L^3 N_{\mathbf{x}})$. But, we control $N_{\mathbf{x}}$ to be bounded through $\rho_{\mathbf{x}}$, so that the total cost in calculating $\psi_I^{[\beta]}(\mathbf{x})$ for all $\mathbf{x}_I$'s in the support of window function at $\mathbf{x}$ will be of $\mathrm{O}(L^5)$.

(3) The cost in computation of the singular function $S_\Gamma^{[\beta]}(\mathbf{x})$ depends on searching the projection point $\bar{\mathbf{x}}_\Gamma$ for a given $\bar{\mathbf{x}}$. In fact, the operation count to calculate $b_\Gamma(\mathbf{x}, \bar{\mathbf{x}})$ is of $\mathrm{O}(N^{1-\frac{1}{d}})$ for each $\bar{\mathbf{x}}$ where N is the number of total nodes in Λ. Therefore, the extrinsic meshfree approximations are calculated with complexity of order $\mathrm{O}(N^{2-\frac{1}{d}})$ for each $\mathbf{x}$.

The extrinsic meshfree approximations derived have the following salient features:

P1. The extrinsic meshfree approximation is composed of two parts. One part possesses the exact singularity for the normal derivative across the interface, and another part is the regular approximation. This property makes the derivative approximations accurate.

P2. It approximates a function separately on the regular and singular regions. The singular effect from the interface is transmitted directly to the singular region and then spreads into the whole domain through the overlapped influence region of the two separated domains. Due to this feature, the diagonal dominance of the discretized system is ensured.

P3. It contains two types of coefficients. $\{u_I\}$ in the regular part is of discrete type while $\left[\frac{\partial u}{\partial n}\right]_{\mathbf{x}_\Gamma}$ in the singular part can be regarded as a coefficient of function type defined on the singular region Ω^{S}.

P4. For any set $\{u_I\}$ and β, $|\beta| \leqslant m$, the regular part $\sum_{\mathbf{x}_I \in \Lambda} u_I \psi_I^{[\beta]}(\mathbf{x})$ of the extrinsic meshfree approximation is continuous on the singular region Ω^{S} including Γ. Because of this property, the extrinsic meshfree approximation becomes flexible in treating interface discontinuity problems.

P5. All polynomials up to approximation order m are exactly reproduced, i.e.,

$$\mathscr{D}_h^\beta u(\mathbf{x}) = D_{\mathbf{x}}^\beta u(\mathbf{x}), \quad \mathbf{x} \in \Omega, \quad |\beta| \leqslant m \tag{27}$$

when $u(x)$ is a polynomial up to order m. In fact, since polynomials are continuously differentiable, we have $\left[\frac{\partial u}{\partial n}\right]_{\mathbf{x}_\Gamma} = 0$.

P6. The jump of the normal derivative across the interface is exactly reproduced

$$\left[(\mathscr{D}_h^{(1,0,\ldots,0)} u, \ldots, \mathscr{D}_h^{(0,\ldots,0,1)} u) \cdot \mathbf{n}\right]_\Gamma = \left[\frac{\partial u}{\partial n}\right]_\Gamma, \tag{28}$$

which is proved in Appendix C. This feature implies that the singular approximation can extract the derivative singularity exactly.

The extrinsic meshfree approximation can be seen as a generalization of the method by Krongauz and Belytschko [12]. As a matter of fact, looking into the extrinsic meshfree approximation (24), the coefficient attached at the singular part equals the jump values of the normal derivative at the projection point of the space variable $\mathbf{x}$ to the interface. The derivative singularity of $u(\mathbf{x})$ is exactly extracted by this coefficient attributed to the wedge function. This is why the extrinsic meshfree approximation should produce outstandingly sharp first order derivatives.

3. Point collocation schemes using the extrinsic meshfree approximation

In most cases, the normal derivative jumps across the interface are not known a priori. When the normal derivative jumps are given in advance, the approximation formula (24) can be easily implemented in the meshfree point collocation method without adding degrees of freedom. In contrast to this case, if the normal derivative jump is unknown, then how to discretize the function $\left[\frac{\partial u}{\partial n}\right]_{\mathbf{x}_\Gamma}$ in (24) must be considered. Although this can be accomplished through modeling of the interface, it is only used for the purpose of function evaluation on the interface. The relationship between the normal derivative jump across the interface and the interface conditions enables us to obtain the unknown function coefficient $\left[\frac{\partial u}{\partial n}\right]_\Gamma$ on the interface as a part of the solution.

In the immersed interface method by LeVeque and Li [13], the derivative jumps across the interface are inserted explicitly into the finite difference discretization of the partial differential equations and accurate integrations of the layer singular sources are obtained. In our method, the βth order singular shape function represents the discontinuities implicitly, so that the point collocation discretization using it reflects the normal derivative jump across the interface effectively.

For modeling of the interface, we introduce the linear interface elements $\mathscr{T}_\Gamma \equiv \{e_K | K = 1, \ldots, N_e\}$. In the regime of the interface element approximation on Γ, every element e_K consists of two end points, a consistent orientation, and two linear basis functions. Let $\Lambda^\Gamma \equiv \{\mathbf{x}_I^\Gamma \in \Gamma | I = 1, \ldots, N_p\}$ be the set of all end points of elements in $\mathscr{T}_\Gamma$ and $\{N_K(\mathbf{x}) | K = 1,\ldots,N_p\}$ be the set of linear interface element basis functions. Based on this setting as shown in Fig. 3, the approximated interface can be denoted by $\Gamma^h \equiv \bigcup_{K=1}^{N_e} e_K$. The interface elements play a role not only in defining the interface Γ but also in evaluating $\left[\frac{\partial u}{\partial n}\right]_\Gamma$. Certainly, the projection map $\mathbf{x}_\Gamma \equiv \mathrm{proj}_\Gamma(\mathbf{x})$ and the map $\mathbf{n}_\Gamma(\mathbf{x})$ for given $\mathbf{x} \in \Omega^S$ are affected by the interface modeling. Fig. 3 describes the situation on the discretized interface as explained in the above. We will use often the symbol Γ instead of Γ^h if there will be no confusion.

For the meshfree point collocation method, assume $\Lambda = \Lambda_o \cup \Lambda_b$ where Λ_o and Λ_b are disjoint sets of nodes, interior nodes and boundary nodes, respectively. For convenience, uniform nodes are used for both problems, the Poisson problem with a known jump and second order elliptic problems with discontinuous coefficients and/or layer source singularity on the interface. However, to show there is little difference in convergence rates even when using irregularly distributed nodes, a numerical example is added in the last Section 3.3.

From now on, to measure the errors for the numerical solutions in point collocation methods, we define the semi L^∞-norm on the set of nodes Λ for any $v(\mathbf{x}) \in C^0(\overline{\Omega})$ as follows:

$$\|v\|_{L^\infty} = \sup_{\mathbf{x}_I \in \Lambda} |v(\mathbf{x}_I)|. \tag{29}$$

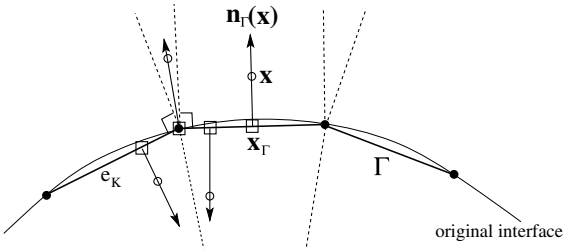

Fig. 3. Illustration of the maps $\bar{\mathbf{x}}_\Gamma \equiv \mathrm{proj}_\Gamma(\bar{\mathbf{x}})$ and $\mathbf{n}_\Gamma(\bar{\mathbf{x}}) \equiv \frac{\mathbf{x}-\bar{\mathbf{x}}_\Gamma}{|\mathbf{x}-\bar{\mathbf{x}}_\Gamma|}$ in case of the discretized interface Γ.

3.1. Elliptic problem with a singular layer source on the interface

Let us consider the Poisson problem with a layer source distributed on the interface. This is a case where the normal derivative jump condition across the interface Γ is known. The problem is written as follows:

$$\Delta u = f, \quad \text{in } \Omega \setminus \Gamma, \tag{30}$$

$$u|_{\partial\Omega} = u^{\partial\Omega}, \tag{31}$$

$$\begin{cases} [u]_\Gamma = 0, \\ \left[\frac{\partial u}{\partial n}\right]_\Gamma = g, \end{cases} \tag{32}$$

where $\Gamma \subset \Omega$ represents the interface, $u^{\partial\Omega}$ and g are known a priori, and the function $f(\mathbf{x})$ is allowed to have discontinuities across the interface.

To obtain the numerical solution, the derivative approximations of the numerical solution and the point collocation scheme for the governing equations are used in the following manner since we know $\left[\frac{\partial u}{\partial n}\right]_\Gamma = g$:

$$\mathscr{D}_h^\beta u^h(\mathbf{x}) = \frac{1}{2} g(\mathrm{proj}_\Gamma(\mathbf{x}))\chi_{\Omega^s}(\mathbf{x}) S_\Gamma^{[\beta]}(\mathbf{x}) + \sum_{\mathbf{x}_I \in \Lambda} u_I \psi_I^{[\beta]}(\mathbf{x}), \quad 0 \leqslant \beta \leqslant m, \tag{33}$$

$$\begin{cases} (\mathscr{D}_h^{(2,0)} + \mathscr{D}_h^{(0,2)}) u^h(\mathbf{x}_I) = f(\mathbf{x}_I), & \mathbf{x}_I \in \Lambda_o, \\ u^h(\mathbf{x}_I) = u^{\partial\Omega}(\mathbf{x}_I), & \mathbf{x}_I \in \Lambda_b. \end{cases} \tag{34}$$

The approximation rules (33) to derivatives of u are applied. We have to take care of the argument of the function g in (33). Rearranging the collocation equations in (34), the term keeping the known jump $g(\mathbf{x}_\Gamma)$ can be separated and placed with the forcing term as follows:

$$\sum_{\mathbf{x}_J \in \Lambda} u_J (\psi_J^{[(2,0)]}(\mathbf{x}_I) + \psi_J^{[(0,2)]}(\mathbf{x}_I)) = f(\mathbf{x}_I) + \frac{1}{2} g(\mathbf{x}_{I\Gamma}) \chi_{\Omega^s}(\mathbf{x}_I)(S_\Gamma^{[(2,0)]}(\mathbf{x}_I) + S_\Gamma^{[(0,2)]}(\mathbf{x}_I)), \quad \mathbf{x}_I \in \Lambda_o, \tag{35}$$

$$\sum_{\mathbf{x}_J \in \Lambda} u_J \psi_J^{[(0,0)]}(\mathbf{x}_I) = u^{\partial\Omega}(\mathbf{x}_I) + \frac{1}{2} g(\mathbf{x}_{I\Gamma}) \chi_{\Omega^s}(\mathbf{x}_I) S_\Gamma^{[(0,0)]}(\mathbf{x}_I), \quad \mathbf{x}_I \in \Lambda_b. \tag{36}$$

This means that the singular source term in the partial differential equation is completely discretized by the meshfree point collocation scheme. Suppose $\mathbf{u}^h$ is the nodal coefficient vector, i.e., $\mathbf{u}^h = \{u_I\}$ and the discrete equations in (35) and (36) can be rewritten as the following matrix equation:

$$\begin{bmatrix} \mathbf{A}^R \\ \mathbf{B}^R \end{bmatrix} [\mathbf{u}^h] = \begin{bmatrix} \mathbf{F} \\ \mathbf{U}^{\partial\Omega} \end{bmatrix} + \begin{bmatrix} \mathbf{S}^\Gamma \\ \mathbf{S}^{\partial\Omega} \end{bmatrix}, \tag{37}$$

where each matrix appearing in the above is given below:

$\mathbf{u}^h$		$\mathbf{x}_J \in \Lambda$
$\mathbf{A}^R$	$\mathbf{x}_I \in \Lambda_o$	$\psi_J^{[(2,0)]}(\mathbf{x}_I) + \psi_J^{[(0,2)]}(\mathbf{x}_I)$
$\mathbf{B}^R$	$\mathbf{x}_I \in \Lambda_b$	$\psi_J^{[(0,0)]}(\mathbf{x}_I)$

$\mathbf{F}$	$\mathbf{x}_I \in \Lambda_o$	$f(\mathbf{x}_I)$
$\mathbf{U}^{\partial\Omega}$	$\mathbf{x}_I \in \Lambda_b$	$u^{\partial\Omega}(\mathbf{x}_I)$
$\mathbf{S}^\Gamma$	$\mathbf{x}_I \in \Lambda_o$	$\frac{1}{2} g(\mathrm{proj}_\Gamma(\mathbf{x}_I))\chi_{\Omega^s}(\mathbf{x}_I)(S_\Gamma^{[(2,0)]}(\mathbf{x}_I) + S_\Gamma^{[(0,2)]}(\mathbf{x}_I))$
$\mathbf{S}^{\partial\Omega}$	$\mathbf{x}_I \in \Lambda_b$	$\frac{1}{2} g(\mathrm{proj}_\Gamma(\mathbf{x}_I))\chi_{\Omega^s}(\mathbf{x}_I) S_\Gamma^{[(0,0)]}(\mathbf{x}_I)$

As seen in the discrete system (37), the jump condition for the normal derivative across Γ eventually results in the discrete singular source term explicitly. This means that the right hand side term $[\mathbf{S}^\Gamma, \mathbf{S}^{\partial\Omega}]^T$ in (37) is the expression of the layer delta source on Γ in terms of the pointwise discretization. Moreover, all geometric effects related to the interface are contained entirely in this term.

The convergence for the meshfree point collocation scheme without interfacial discontinuities has been proved by Kim and Liu [10] recently. The numerical example below shows the same convergence rate as the regular problem, which is predictable due to the completely separated source singularity such as (37).

Let us consider the problem defined on the domain $\Omega \equiv [0,4]\times[0,4]$ with a singular source on the interface $\Gamma \equiv \{\mathbf{x} = (x,y) \in \Omega \| \mathbf{x} - \mathbf{x}_c| = 1\}$ where $\mathbf{x}_c = (2,2)$. Assume the data $f(\mathbf{x})$ and the singular source strength $g(\mathbf{x})$ are given as follows:

$$f(\mathbf{x}) = \begin{cases} 0, & |\mathbf{x} - \mathbf{x}_c| < 1, \\ 8(x-2), & |\mathbf{x} - \mathbf{x}_c| > 1, \end{cases} \tag{38}$$

$$g(\mathbf{x}) = 2(x-2), \quad \mathbf{x} \in \Gamma. \tag{39}$$

The boundary value $u^{\partial\Omega}(\mathbf{x})$ on $\partial\Omega$ is taken from the exact solution satisfying (30) and (32):

$$u(\mathbf{x}) = \begin{cases} x-2, & |\mathbf{x} - \mathbf{x}_c| \leqslant 1, \\ (x-2)|\mathbf{x} - \mathbf{x}_c|^2, & |\mathbf{x} - \mathbf{x}_c| > 1. \end{cases} \tag{40}$$

The node distribution is illustrated in Fig. 4 where $\Lambda = \{(ih, jh) | i,j = 0,\ldots,N, h = \frac{4}{N}\}$. In this problem, the interface element approximation of a function is not needed since the normal derivative jump across the interface is given a priori. Necessarily we need the modeling(or defining numerically) of the interface. For simplicity, the numerical interface is defined as a combination of oriented line segments like the interface element e_K as introduced in the beginning of this section. The only purpose of the numerical interface in this problem is to calculate the projection map proj($\mathbf{x}$).

Three discretization models with $N = 20$, 40, and 80 are considered to numerically estimate the decay rates of the relative nodal L^∞ errors of both the extrinsic meshfree approximation and the numerical solution. Fig. 5 shows the convergence rates of the approximations $\mathscr{D}_h^{(0,0)}u(\mathbf{x})$, $(\mathscr{D}_h^{(1,0)}u(\mathbf{x}), \mathscr{D}_h^{(0,1)}u(\mathbf{x}))$, and $\mathscr{D}_h^{(2,0)}u(\mathbf{x}) + \mathscr{D}_h^{(0,2)}u(\mathbf{x})$ for the exact function $u(\mathbf{x})$ in (40). The convergence rates are approximately $O(h^2)$, $O(h)$, and $O(1)$, respectively.

The convergence rate of the error between the numerical solution $u^h(\mathbf{x})$ from the scheme (37) and the exact solution $u(\mathbf{x})$ in (40) stays around $O(h^2)$ within small differences while the convergence rate for the approximated derivative of the numerical solution $u^h(\mathbf{x})$ in the meaning of (33) is almost equal to $O(h)$ as shown in Fig. 6. This result coincides with that of the symmetric discretization method in [6] which produces the second-order accuracy for the essentially same type of Poisson equation, while the boundary condition capturing method in [19] has $O(h^{1.4})$ accuracy.

In finite difference methods, the convergence of the numerical solution for elliptic partial differential equations is critically affected by the truncation error for the differential equations. However, in case of this mesh-

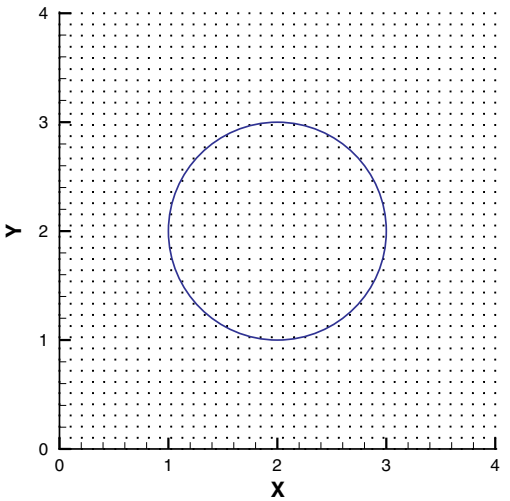

Fig. 4. Example of a node distribution and the interface on which singular layer source is given.

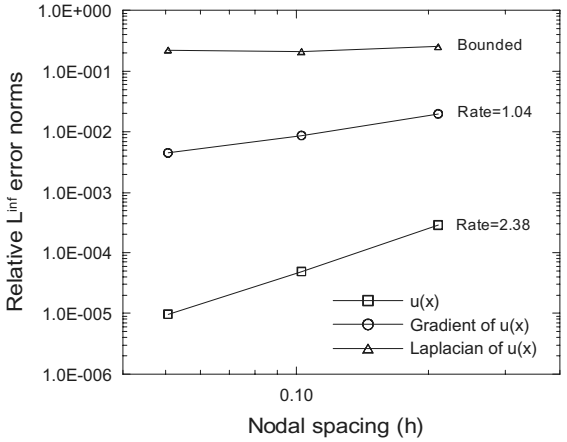

Fig. 5. Convergence rates of the extrinsic meshfree approximation.

free point collocation scheme, the optimal convergence rate is achieved despite the boundedness of the truncation error $\|\Delta u - \Delta^h u\|_{L^\infty}$. To explain this exceptional convergence of the numerical solution in our meshfree point collocation scheme as defined in (37), we should point out that the nodal coefficients u_I's must not be regarded as a nodal value of the solution, i.e., $u_I \neq u(\mathbf{x}_I)$. By doing so, the truncation error is completely removed from the definition of the discretization (35). In Fig. 7, the sharp discontinuities of the derivative of the numerical solution are shown; there is no smearing at the interface. This implies that the extrinsic meshfree approximation (24) completely extracts the derivative jump from the first order derivatives across the interface.

3.2. Elliptic problem with both singular layer source and discontinuous coefficients across the interface

Let us consider the following elliptic problem associated with the singular layer source and the discontinuous coefficients $\kappa(\mathbf{x})$ across the interface Γ which is equivalent to the following problem:

$$\nabla \cdot (\kappa \nabla u) = f, \quad \text{in } \Omega \setminus \Gamma, \tag{41}$$

$$u|_{\partial\Omega} = u^{\partial\Omega}, \tag{42}$$

$$\begin{cases} [u]_\Gamma = 0, \\ \left[\kappa \frac{\partial u}{\partial n}\right]_\Gamma = q^\Gamma, \end{cases} \tag{43}$$

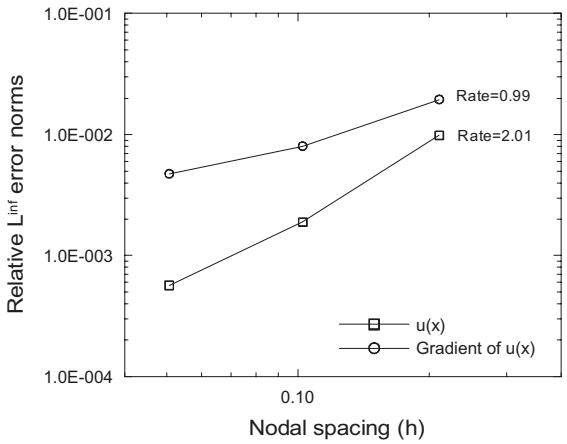

Fig. 6. Convergence rates of the numerical solution.

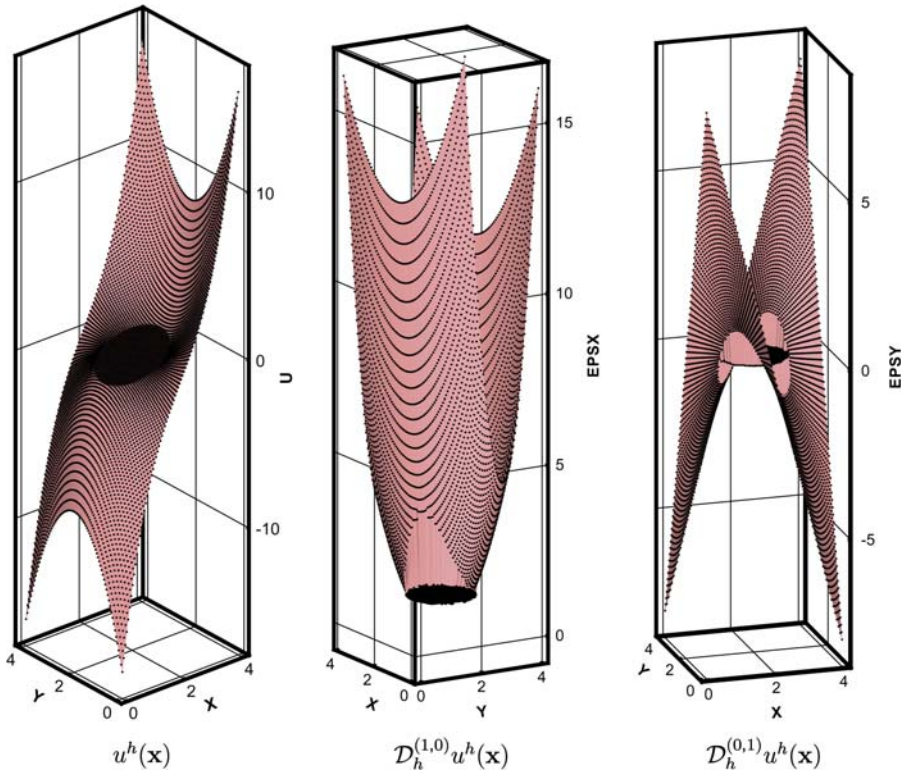

Fig. 7. Numerical solutions.

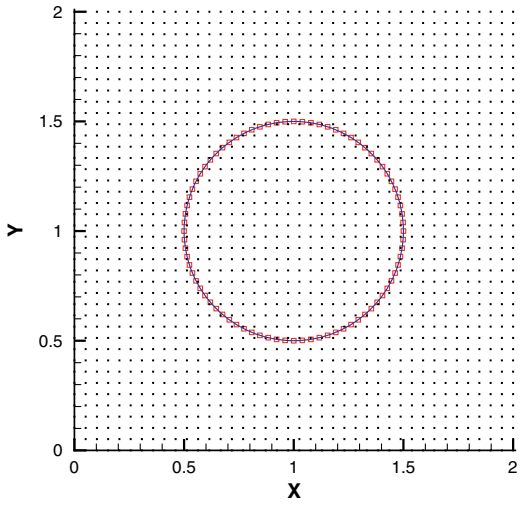

Fig. 8. Typical node distribution and the interface on which the singular layer source is given and across which the coefficients are discontinuous.

where $\Gamma \subset \Omega$ represents the interface, the functions $f(\mathbf{x})$ and $\kappa(\mathbf{x})(>0)$ possibly have jump discontinuities along the interface, and both $u^{\partial\Omega}$ and q^{Γ} are known a priori. It should be stated that $\left[\frac{\partial u}{\partial n}\right]_{\Gamma}$ is not known in this case.

If $\kappa(\mathbf{x})$ is continuous on Γ, then this problem becomes similar to the previous one. This problem is closely related to the single layer source δ_{Γ} along the interface, for example, such as a heat source which is located

at the interface between materials with different conductivities. In order to solve this interface problem using the approximation formula (24), the mapping $\mathscr{I}$ from the pair $(q^\Gamma(\mathbf{x}),u(\mathbf{x}))$ of the source strength and its corresponding solution to the normal derivative jump $\left[\frac{\partial u}{\partial n}\right]_\Gamma$ should be characterized since the jump value $\left[\frac{\partial u}{\partial n}\right]_\Gamma$ is a part of the solution even if the source strength $q^\Gamma(\mathbf{x})$ is known. The mapping $\mathscr{I}$ will be called *the jump map*.

To implement explicitly the jump map which is implicitly defined, we use the product rule for the jumps across the interface: if the functions v and w are defined on both sides of the interface as limit values, then we have

$$[vw]_\Gamma = [v]_\Gamma\langle w\rangle_\Gamma + \langle v\rangle_\Gamma[w]_\Gamma, \tag{44}$$

where the brackets $\langle\cdot\rangle_\Gamma$ and $[\cdot]_\Gamma$ designate the average and the directional difference values on both sides of Γ, respectively, as already mentioned before. Following this rule, the interface condition that $\left[\kappa\frac{\partial u}{\partial n}\right]_\Gamma = q^\Gamma$ can be transformed into the following:

$$[\kappa]_\Gamma\left\langle\frac{\partial u}{\partial n}\right\rangle_\Gamma + \langle\kappa\rangle_\Gamma\left[\frac{\partial u}{\partial n}\right]_\Gamma = q^\Gamma. \tag{45}$$

To discretize the interface jump condition (45), all derivatives appearing in the equation are replaced by the approximated derivatives in (24) except for the term $\left[\frac{\partial u}{\partial n}\right]_\Gamma$ since $\left[\frac{\partial u}{\partial n}\right]_\Gamma$ is unknown and to be determined as a part of the solution.

First of all, if we define the approximated gradient symbols ∇^h and ∇^h_Γ induced from the operator $\mathscr{D}^\beta_h$ such that

$$\nabla^h\psi_I(\mathbf{x}) \equiv (\psi_I^{[(1,0)]}(\mathbf{x}),\psi_I^{[(0,1)]}(\mathbf{x})), \tag{46}$$

$$\nabla^h_\Gamma S_\Gamma(\mathbf{x}) \equiv (S_\Gamma^{[(1,0)]}(\mathbf{x}),S_\Gamma^{[(0,1)]}(\mathbf{x})), \tag{47}$$

then we can calculate the average term in (45) as follows:

$$\begin{aligned}\left\langle\frac{\partial u}{\partial n}\right\rangle_\Gamma &= \left\langle\frac{1}{2}\left[\frac{\partial u}{\partial n}\right]_\Gamma\nabla^h_\Gamma S_\Gamma(\mathbf{x})\cdot\mathbf{n} + \sum_{\mathbf{x}_I\in\mathcal{A}}u_I\nabla^h\psi_I(\mathbf{x})\cdot\mathbf{n}\right\rangle_\Gamma \\ &= \frac{1}{2}\left[\frac{\partial u}{\partial n}\right]_\Gamma\langle\nabla^h_\Gamma S_\Gamma(\mathbf{x})\cdot\mathbf{n}\rangle_\Gamma + \sum_{\mathbf{x}_I\in\mathcal{A}}u_I\langle\nabla^h\psi_I(\mathbf{x})\cdot\mathbf{n}\rangle_\Gamma.\end{aligned} \tag{48}$$

Applying the definition of singular shape function in (25) to the term $\langle\nabla^h_\Gamma S_\Gamma(\mathbf{x})\cdot\mathbf{n}\rangle_\Gamma$, we have

$$\begin{aligned}\langle\nabla^h_\Gamma S_\Gamma(\mathbf{x})\cdot\mathbf{n}\rangle_\Gamma &= \langle(D^{(1,0)}_{\mathbf{x}}b_\Gamma(\mathbf{x},\bar{\mathbf{x}})|_{\bar{\mathbf{x}}=\mathbf{x}},D^{(0,1)}_{\mathbf{x}}b_\Gamma(\mathbf{x},\bar{\mathbf{x}})|_{\bar{\mathbf{x}}=\mathbf{x}})\cdot\mathbf{n}\rangle_\Gamma - \sum_{\mathbf{x}_I\in\mathcal{A}}b_\Gamma(\mathbf{x}_I,\mathbf{x})\langle\nabla^h\psi_I(\mathbf{x})\cdot\mathbf{n}\rangle_\Gamma \\ &= -\sum_{\mathbf{x}_I\in\mathcal{A}}b_\Gamma(\mathbf{x}_I,\mathbf{x})\langle\nabla^h\psi_I(\mathbf{x})\cdot\mathbf{n}\rangle_\Gamma,\end{aligned} \tag{49}$$

since the first term on the right hand side of the first equation must be zero from the properties of (18) and (19). On the other hand, from the continuity of the regular part of the extrinsic meshfree approximation on Γ, the following identity holds

$$\langle\nabla^h\psi_I(\mathbf{x})\cdot\mathbf{n}\rangle_\Gamma = \nabla^h\psi_I(\mathbf{x})\cdot\mathbf{n}, \quad \mathbf{x}\in\Gamma. \tag{50}$$

Inserting (49) into (48) and consecutively the result into the jump condition (45) based on the identity (50), the following relationship between the pair $(q^\Gamma(\mathbf{x}),u(\mathbf{x}))$ and the jump $\left[\frac{\partial u}{\partial n}\right]_\Gamma$ can be derived from the interface condition (48) with the extrinsic meshfree approximation:

$$[\kappa]_\Gamma\sum_{\mathbf{x}_I\in\mathcal{A}}u_I(\nabla^h\psi_I(\mathbf{x}_\Gamma)\cdot\mathbf{n}) + \left[\frac{\partial u}{\partial n}\right]_\Gamma\left(\langle\kappa\rangle_\Gamma - \frac{1}{2}[\kappa]_\Gamma\sum_{\mathbf{x}_I\in\mathcal{A}}b_\Gamma(\mathbf{x}_I,\mathbf{x}_\Gamma)\big(\nabla^h\psi_I(\mathbf{x}_\Gamma)\cdot\mathbf{n}\big)\right) = q^\Gamma. \tag{51}$$

Fortunately, the interface condition (43) is discretized to be (51), so that the jump map $\mathscr{I}$ is defined explicitly by solving the algebraic equation (51) with respect to $\left[\frac{\partial u}{\partial n}\right]_\Gamma$.

Let us derive the point collocation system to simultaneously solve Eqs. (41) and (42) together with the interface condition (51). The strategy in the meshfree point collocation method is to discretize the partial differential Eq. (41) on the interior nodes and the boundary condition (42) on the boundary nodes and to implement the jump map $\mathscr{I}$ in (51) on the interface element nodes. All differential D^β's are replaced by the approximated derivative $\mathscr{D}_h^\beta$ defined in (24). The approximate solution takes the following form:

$$u^h(\mathbf{x}) = \frac{1}{2}\left[\frac{\partial u}{\partial n}\right]_{\mathbf{x}_\Gamma} \chi_{\Omega^S}(\mathbf{x}) S_\Gamma^{[(0,0)]}(\mathbf{x}) + \sum_{\mathbf{x}_I \in \Lambda} u_I \psi_I^{[(0,0)]}(\mathbf{x}), \quad \forall \mathbf{x} \in \Omega. \tag{52}$$

As mentioned before, it has both the unknown composite function $\left[\frac{\partial u}{\partial n}\right]_{\mathbf{x}_\Gamma}$ and the discrete coefficients u_I's. Since the function $\left[\frac{\partial u}{\partial n}\right]_{\mathbf{x}_\Gamma}$ should be interpreted as a composition of two functions such that

$$\left[\frac{\partial u}{\partial n}\right]_{\mathbf{x}_\Gamma} = \left[\frac{\partial u}{\partial n}\right]_\Gamma \circ \operatorname{proj}_\Gamma(\mathbf{x}), \quad \mathbf{x} \in \Omega^S, \tag{53}$$

we take the interface element approximation only for the function $\left[\frac{\partial u}{\partial n}\right]_\Gamma$ defined on Γ:

$$\left[\frac{\partial u}{\partial n}\right]_\Gamma = \sum_{I=1}^{N_p} g_I N_I(\mathbf{x}), \quad \mathbf{x} \in \Gamma, \tag{54}$$

where $N_I(\mathbf{x})$ is the 1D linear interface element basis function at $\mathbf{x}_I^\Gamma \in \Lambda^\Gamma$. As a result, the function coefficient can be discretized as follows:

$$\left[\frac{\partial u}{\partial n}\right]_{\mathbf{x}_\Gamma} = \sum_{I=1}^{N_p} g_I N_I(\operatorname{proj}_\Gamma(\mathbf{x})), \quad \mathbf{x} \in \Omega^S. \tag{55}$$

To obtain the discrete system for the unknowns g_I and u_I,

(1) Eq. (41) is discretized at every interior node in Λ_o: for any $\mathbf{x}_I \in \Lambda_o$,

$$\sum_{\mathbf{x}_J \in \Lambda^\Gamma} g_J N_J(\operatorname{proj}_\Gamma(\mathbf{x}_I)) \chi_{\Omega^S}(\mathbf{x}_I)\left(\frac{1}{2} L_\Gamma^h S_\Gamma(\mathbf{x}_I)\right) + \sum_{\mathbf{x}_J \in \Lambda} u_J L^h \psi_J(\mathbf{x}_I) = f(\mathbf{x}_I), \tag{56}$$

where $L_\Gamma^h S_\Gamma = \kappa(S_\Gamma^{[(2,0)]} + S_\Gamma^{[(0,2)]}) + \nabla\kappa \cdot \nabla_\Gamma^h S_\Gamma$ and $L^h\psi_J = \kappa(\psi_J^{[(2,0)]} + \psi_J^{[(0,2)]}) + \nabla\kappa \cdot \nabla^h \psi_J$ in which the gradient symbols in (46) and (47) are used.

(2) The discretization of the boundary condition (42) is provided for any $\mathbf{x}_I \in \Lambda_B$ as follows:

$$\sum_{\mathbf{x}_J \in \Lambda} u_J \psi_J^{[(0,0)]}(\mathbf{x}_I) + \sum_{\mathbf{x}_J \in \Lambda^\Gamma} g_J N_J(\operatorname{proj}_\Gamma(\mathbf{x}_I)) \chi_{\Omega^S}(\mathbf{x}_I)\left(\frac{1}{2} S_\Gamma^{[(0,0)]}(\mathbf{x}_I)\right) = u^{\partial\Omega}(\mathbf{x}_I). \tag{57}$$

(3) The discretization of the jump map $\mathscr{I}$ using (43) and the property that $N_I(\mathbf{x}_J) = \delta_{IJ}$ for all $\mathbf{x}_I$ and $\mathbf{x}_J$ in Λ^Γ becomes the following for any $\mathbf{x}_I \in \Lambda^\Gamma$:

$$\sum_{\mathbf{x}_J \in \Lambda} u_J [\kappa]_{\mathbf{x}_I} (\nabla^h \psi_J(\mathbf{x}_I) \cdot \mathbf{n}) + \sum_{\mathbf{x}_J \in \Lambda^\Gamma} g_J \delta_{IJ}\left(\langle\kappa\rangle_{\mathbf{x}_I} - \frac{1}{2}[\kappa]_{\mathbf{x}_I} \sum_{\mathbf{x}_K \in \Lambda} b_\Gamma(\mathbf{x}_K, \mathbf{x}_I)(\nabla^h \psi_K(\mathbf{x}_I) \cdot \mathbf{n})\right) = q^\Gamma(\mathbf{x}_I). \tag{58}$$

Assembling all discretizations 1, 2, and 3 in the above, we finally obtain the system for $\mathbf{g} \equiv \{g_I\}$ and $\mathbf{u}^h \equiv \{u_I\}$:

$$\left[\begin{array}{c|c} \mathbf{A}^R & \mathbf{A}^S \\ \hline \mathbf{B}^R & \mathbf{B}^S \end{array}\right]\left[\begin{array}{c} \mathbf{u}^h \\ \hline \mathbf{g} \end{array}\right] = \left[\begin{array}{c} \mathbf{F} \\ \hline \mathbf{U}^{\partial\Omega} \end{array}\right], \quad \left[\begin{array}{c|c} \mathbf{I}^R & \mathbf{I}^S \end{array}\right]\left[\begin{array}{c} \mathbf{u}^h \\ \hline \mathbf{g} \end{array}\right] = \left[\mathbf{Q}\right], \tag{59}$$

where the submatrices $\mathbf{A}^R$, $\mathbf{A}^S$, $\mathbf{B}^R$, $\mathbf{B}^S$, $\mathbf{I}^R$, $\mathbf{I}^S$ and vectors $\mathbf{F}$, $\mathbf{U}^{\partial\Omega}$, $\mathbf{Q}$ are derived from the point collocation discretization to have the following forms:

	$\mathbf{u}^h$		$\mathbf{x}_J \in \Lambda$
$\mathbf{A}^{\mathrm{R}}$		$\mathbf{x}_I \in \Lambda_{\mathrm{o}}$	$\kappa(\mathbf{x}_I)\Delta^h\psi_J(\mathbf{x}_I) + \nabla\kappa(\mathbf{x}_I)\cdot\nabla^h\psi_J(\mathbf{x}_I)$
$\mathbf{B}^{\mathrm{R}}$		$\mathbf{x}_I \in \Lambda_b$	$\psi_J^{[(0,0)]}(\mathbf{x}_I)$
$\mathbf{I}^{\mathrm{R}}$		$\mathbf{x}_I \in \Lambda^\Gamma$	$[\kappa]_{\mathbf{x}_I}(\nabla^h\psi_J(\mathbf{x}_I)\cdot\mathbf{n})$
	$\mathbf{g}$		$\mathbf{x}_J \in \Lambda^\Gamma$
$\mathbf{A}^{\mathrm{S}}$		$\mathbf{x}_I \in \Lambda_{\mathrm{o}}$	$\frac{1}{2}\chi_{\Omega^{\mathrm{s}}}(\mathbf{x}_I)N_J(\mathrm{proj}_\Gamma(\mathbf{x}_I))(\kappa(\mathbf{x}_I)\Delta_\Gamma^h S_\Gamma(\mathbf{x}_I) + \nabla\kappa(\mathbf{x}_I)\cdot\nabla_\Gamma^h S_\Gamma(\mathbf{x}_I))$
$\mathbf{B}^{\mathrm{S}}$		$\mathbf{x}_I \in \Lambda_b$	$\frac{1}{2}\chi_{\Omega^{\mathrm{s}}}(\mathbf{x}_I)N_J(\mathrm{proj}_\Gamma(\mathbf{x}_I))S_\Gamma^{[(0,0)]}(\mathbf{x}_I)$
$\mathbf{I}^{\mathrm{S}}$		$\mathbf{x}_I \in \Lambda^\Gamma$	$\delta_{IJ}(\langle\kappa\rangle_{\mathbf{x}_I} - \frac{1}{2}[\kappa]_{\mathbf{x}_I}\sum_{\mathbf{x}_K\in\Lambda} b_\Gamma(\mathbf{x}_K,\mathbf{x}_I)(\nabla^h\psi_K(\mathbf{x}_I)\cdot\mathbf{n}))$

$\mathbf{F}$	$\mathbf{x}_I \in \Lambda_{\mathrm{o}}$	$f(\mathbf{x}_I)$
$\mathbf{U}^{\partial\Omega}$	$\mathbf{x}_I \in \Lambda_b$	$u^{\partial\Omega}(\mathbf{x}_I)$
$\mathbf{Q}$	$\mathbf{x}_I \in \Lambda^\Gamma$	$q^\Gamma(\mathbf{x}_I)$

Remark 3. The matrix $\mathbf{I}^{\mathrm{S}}$ in (59) is a diagonal matrix. With its inverse, we can eliminate the unknown $\mathbf{g}$ in the system (59). Therefore, the degree of freedom for the system reduces to the number of domain nodes only.

For the numerical experiment of the meshfree point collocation scheme proposed in (59), we assume $\Omega = [0,2]\times[0,2]$ and $\Gamma = \{\mathbf{x}\in\Omega \,|\, |\mathbf{x}-\mathbf{x}_c| = \frac{1}{2}\}$ when $\mathbf{x}_c = (1,1)$. In the computations, we use the uniform node arrangement as in the previous example. However, unlike the previous numerical example, the linear interface element approximation is used to calculate the unknown jump function $\left[\frac{\partial u}{\partial n}\right]_\Gamma$ (see Fig. 8). In the problem of (41)–(43), the material coefficient $\kappa(\mathbf{x})$ and the force term $f(\mathbf{x})$ in (41) is chosen as follows:

$$\kappa(\mathbf{x}) = \begin{cases} |\mathbf{x}-\mathbf{x}_c|^2 + 1, & |\mathbf{x}-\mathbf{x}_c| \leqslant \frac{1}{2}, \\ \kappa_+, & |\mathbf{x}-\mathbf{x}_c| > \frac{1}{2}, \end{cases} \tag{60}$$

$$f(\mathbf{x}) = 8|\mathbf{x}-\mathbf{x}_c|^2 + 4, \tag{61}$$

where κ_+ is a positive constant.

Then, the Dirichlet data $u^{\partial\Omega}(\mathbf{x})$ in (42) is imposed on $\partial\Omega$ by the exact solution of this problem with the source strength $q^\Gamma = 2C$ for some constant C in (43) written as follows:

$$u(\mathbf{x}) = \begin{cases} |\mathbf{x}-\mathbf{x}_c|^2, & |\mathbf{x}-\mathbf{x}_c| \leqslant \frac{1}{2}, \\ \frac{1}{4}\left(1 - \frac{9}{8\kappa_+}\right) + \frac{|\mathbf{x}-\mathbf{x}_c|^2}{2\kappa_+}(|\mathbf{x}-\mathbf{x}_c|^2 + 2) + \frac{C}{\kappa_+}\log 2|\mathbf{x}-\mathbf{x}_c|, & |\mathbf{x}-\mathbf{x}_c| > \frac{1}{2}. \end{cases} \tag{62}$$

This example stems from [13]. In this problem, the exact jump of the normal derivative of the solution is constant along the interface, i.e., $\left[\frac{\partial u}{\partial n}\right]_\Gamma = \frac{5+8C}{4\kappa_+} - 1$. It should be calculated as a part of the solution. The numerical calculations are performed with $C = 0.1$ and $\kappa_+ = 10$, 100. Fig. 9 shows the convergence rates for the numerical solutions $u^h(\mathbf{x})$, the approximated gradient $(\mathscr{D}_h^{(1,0)}u^h(\mathbf{x}), \mathscr{D}_h^{(0,1)}u^h(\mathbf{x}))$, and the approximated jump $\mathbf{g}$ for the cases when $\kappa_+ = 10$ and $\kappa_+ = 100$, respectively.

When $\kappa_+ = 10$, the convergence rates of the solution, the gradient, and the normal derivative jump on Γ are $\mathrm{O}(h^{1.76})$, $\mathrm{O}(h^{1.23})$, and $\mathrm{O}(h^{0.69})$, respectively. The numerical result shows that the convergence rate for the gradient of the solution is better than optimal convergence $\mathrm{O}(h)$. For reference, the weak formulation method in [8] for the same problem ($\kappa_+ = 10, C = 0.1$) has obtained $\mathrm{O}(h^2)$ and $\mathrm{O}(h^{1.5})$ convergence rates for u^h and ∇u^h, respectively. Furthermore, as the value of $[\kappa(\mathbf{x})]$ becomes larger($\kappa_+ = 100$), consistent convergence rates are obtained as shown in Fig. 9. This implies that the proposed method seems to be robust as $[\kappa]_\Gamma$ becomes bigger. Besides, Table 1 shows that the accuracy and the robustness are not affected by the

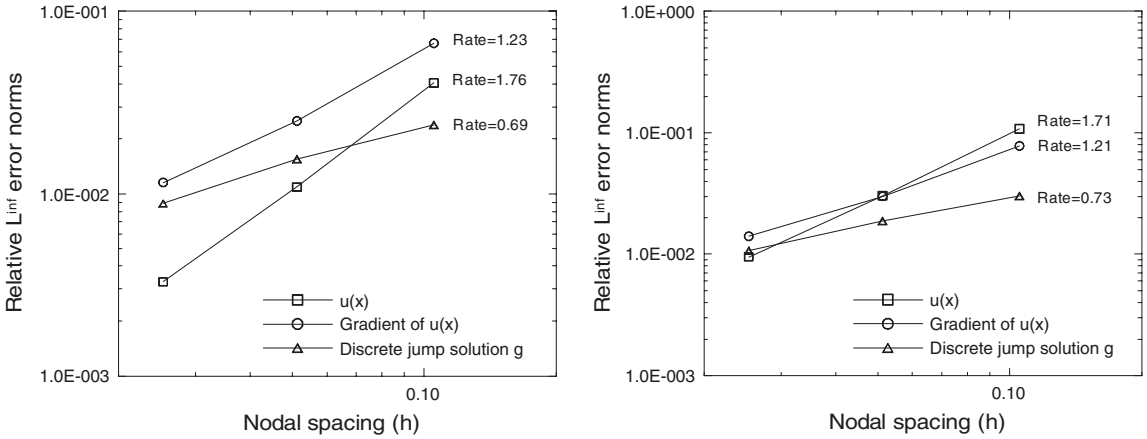

Fig. 9. Convergence rates on the numerical solutions when $\kappa_+ = 10$ and $\kappa_+ = 100$: $u^h(\mathbf{x})$, the approximated gradient $(\mathscr{D}_h^{(1,0)}u^h(\mathbf{x}), \mathscr{D}_h^{(0,1)}u^h(\mathbf{x}))$, and the normal derivative jump $\mathbf{g}$.

Table 1
The independency of the numerical scheme on the number N_p of interface defining points for the node model 20×20

N_p	$\|\mathbf{g} - \left[\frac{\partial u}{\partial n}\right]_\Gamma\|_{L^\infty(\Lambda^\Gamma)}$	$\|u^h - u\|_{L^\infty(\Lambda)}$	$\|\nabla^h u^h - \nabla u\|_{L^\infty(\Lambda)}$
40	2.3896×10^{-2}	4.0532×10^{-2}	6.6819×10^{-2}
80	2.1938×10^{-2}	3.8450×10^{-2}	6.3262×10^{-2}
160	2.1619×10^{-2}	3.8311×10^{-2}	6.1748×10^{-2}
320	2.1534×10^{-2}	3.8167×10^{-2}	6.1736×10^{-2}

number of interface elements on Γ if the number is greater than about 2 times the square root of the total number of nodes.

For $C = 0.1$ and $\kappa_+ = 10$, the numerically calculated jumps of the normal derivative across the interface are depicted in Fig. 14 and compared with the exact jump $\left[\frac{\partial u}{\partial n}\right]_\Gamma = -\frac{171}{200}$. For $C = 0.1$, Figs. 10–13 illustrate the numerical solution and the extrinsic meshfree derivatives when $\kappa_+ = 10$ and $\kappa_+ = 100$, respectively. The sharp feature of our extrinsic meshfree derivatives is seen well.

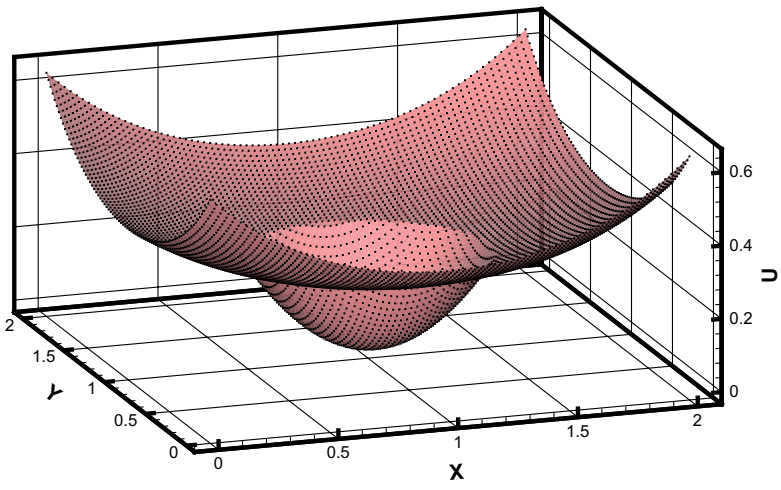

Fig. 10. Numerical solution $u^h(\mathbf{x})$ when $\kappa_+ = 10$ and $C = 0.1$ (80×80 node model).

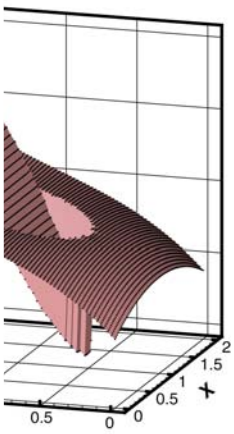

$^{h}(\mathbf{x})$

80×80 node model).

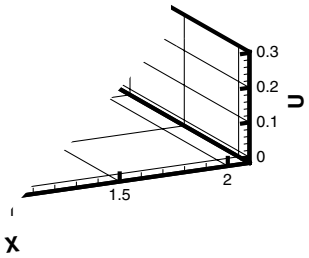

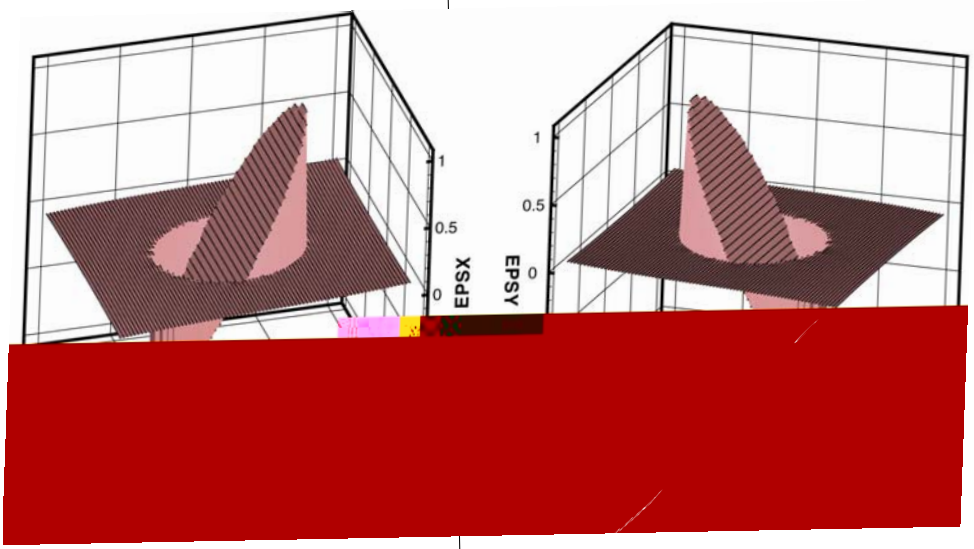

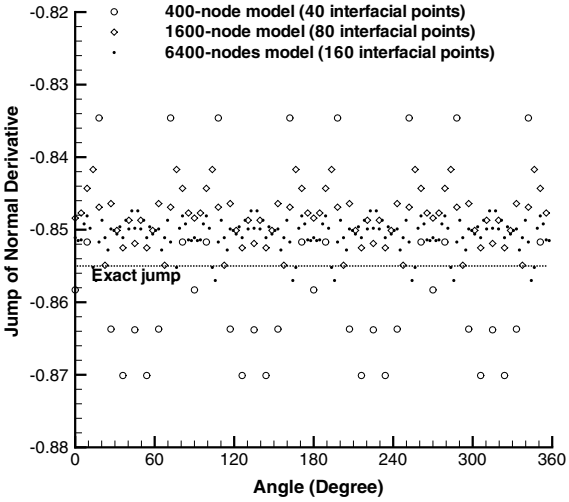

Fig. 14. Comparison of exact and the numerical derivative jump g when $C = 0.1$ and $\kappa_+ = 10$ for different refinements.

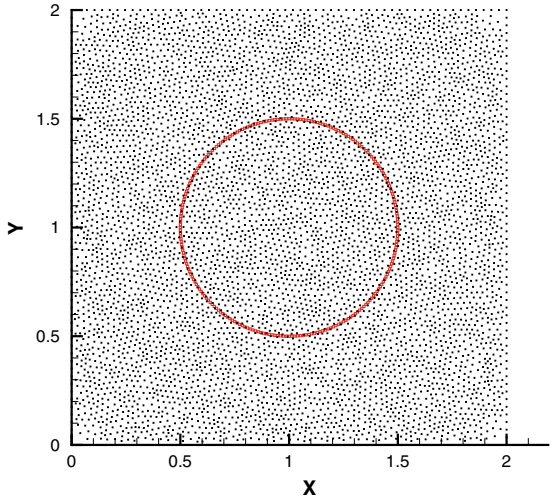

Fig. 15. Illustration of the typical irregular node distribution used in calculation: the number of the interface defining points, i.e., N_p is usually taken as around $4 \times \sqrt{\text{the number of nodes}}$.

3.3. Example on irregularly distributed nodes

This subsection is devoted to emphasizing that this method is meshfree and the calculation results on irregular nodes have little difference compared to those on uniformly distributed nodes and are even better in the specific example employed here.

We adopt the same example ($\kappa_+ = 10, C = 0.1$) as in Section 3.2 to compare its numerical results on irregularly distributed nodes for the interface problem governed by Eqs. (41)–(43) with those on uniform nodes. The typical node distribution and interface model are illustrated in Fig. 15. All irregular node models used in calculation have 815, 3075, and 6212 nodes.

Fig. 16 shows the convergence rates of both the extrinsic meshfree approximations and the numerical solutions on these node models, which are located at the left and right sides of the figure, respectively. Dashed lines correspond to the exact convergence orders, O(1), O(h^1), and O(h^2). As for the extrinsic mesh-

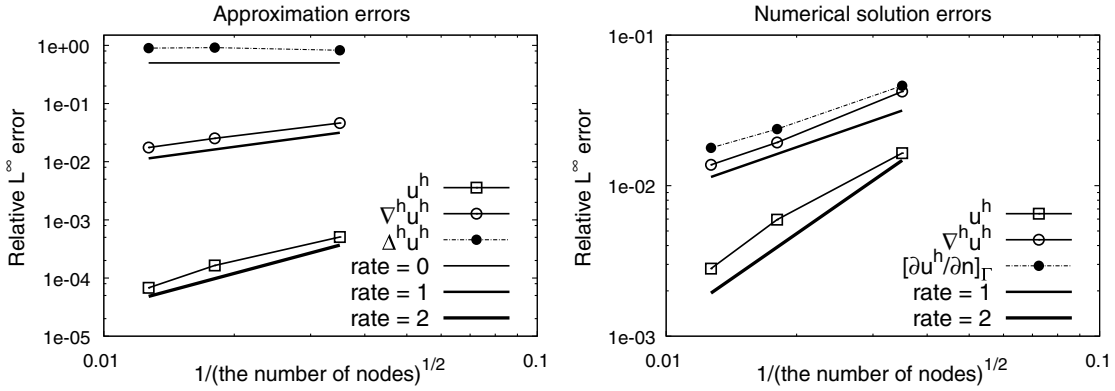

Fig. 16. On irregular node distributions, convergence rates for the extrinsic meshfree approximation (Left) and the numerical solution (Right).

free approximations, the same orders of convergence are shown as for the uniform model case, for example, the relative errors of u^h, $\nabla^h u^h$, and $\Delta^h u^h$ on nodes have $O(h^2)$, $O(h)$, and $O(1)$ convergence rates, respectively. Those results are anticipated from extracting layer singularities up to first order derivatives in this paper.

More interesting results are the right hand side of Fig. 16. Comparing with the left hand side ($\kappa_+ = 10, C = 0.1$) of Fig. 9 in the uniform node case, the calculation on irregular nodes seems to produce better results. In general, it has been thought that uniform model yields the best numerical solution in FDM as well as FEM. However, in the meshfree point collocation scheme equipped with the interface treatment, this rule does not hold at least for our specific example. Thinking about the reason, in case of irregular node distribution as seen in Fig. 15, the structure of distributed nodes near each point on the interface Γ is same while, on uniform nodes, the directivity of nodes is different point by point on interface. Thus, in case of uniform node distribution, all projection points of $\Omega^S \cap \Lambda$ to Γ are non-uniform on the interface. Since the error of the numerical solution is governed by that on the interface, the uniform property of the projection points on Γ can explain why the better convergence occurs for the irregular node case.

The numeral solutions for the 6212 irregular node model are shown in Fig. 17. The sharp solutions near the interface are still preserved. Particularly, we can see that the first order derivatives have no smearing on interface at all.

Lastly, we consider an example with complex interface(non-convex) as shown in Fig. 18 for the purpose of investigating extendability of our scheme to practical problems. The issue on the variation of the conjugate gradient method (CGM) iterations as the number of interface nodes increases is addressed in Table 2 where

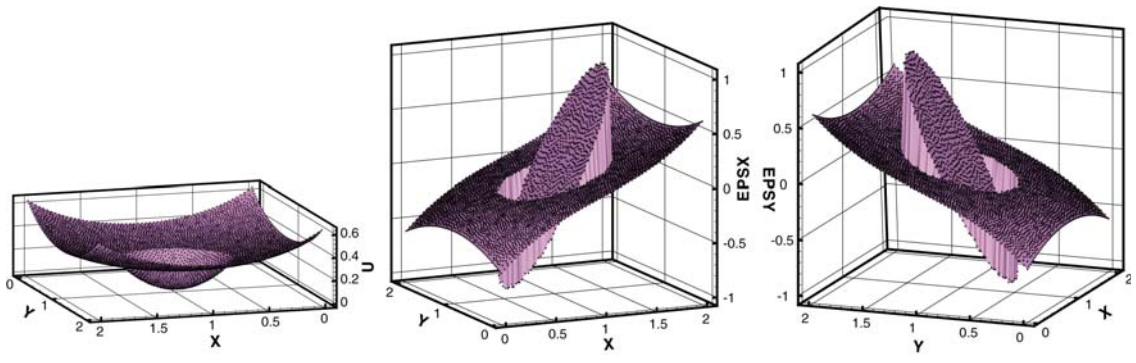

Fig. 17. Figures of the numerical solutions ($\kappa_+ = 10, C = 0.1$) calculated on the irregular nodes: u^h, $\mathscr{D}_h^{(1,0)} u^h$, and $\mathscr{D}_h^{(0,1)} u^h$ in order.

the stopping tolerance is set to be $O(10^{-12})$. According to the table, the CGM iteration numbers seem to be bounded even if the number of interface defining points N_Γ increases under the fixed number N of total nodes in Λ. This fact implies the ellipticity of system matrix is not affected by the interface discretization. The numerical solutions for the complex interface are depicted in Fig. 10, which shows the sharp approximations of the first order derivatives as we anticipated.

However, the real world problems involve more complicated interfaces than our examples. For example, interface can have end points, multiple junctions ,or both. The singularities induced from such kinds of interfaces must be resolved before applying our method. Therefore, further study is needed.

4. Conclusions

New approximations for the interfacial derivative discontinuities across the interface for meshfree methods are proposed. Using the point collocation strategy based on these new approximations, elliptic partial differential equations with discontinuous coefficients are solved effectively. The accuracy of the extrinsic meshfree approximations is shown through numerical examples. The point collocation scheme combined with the extrinsic meshfree approximations provides robust numerical results for the modeling of interfaces and accu-

$$|R_m(\mathbf{y}-\mathbf{x};\mathbf{x})| \leqslant \left(\sup_{|\alpha|=m+1} \sup_{\mathbf{w}\in\Omega\setminus\Gamma} |D^\alpha u(\mathbf{w})| \sum_{|\alpha|=m+1} \frac{1}{\alpha!} \right) |\mathbf{y}-\mathbf{x}|^{m+1}. \tag{66}$$

Proof of Lemma 4. Let Γ be a smooth interface in an open domain $\Omega \subset \mathbb{R}^d$ and $\mathbf{x}$ be a point on Γ. Assume u is a function in $C_B^{m+1}(\Omega \setminus \Gamma)$ and $\mathbf{z}$ is a point satisfying $L(\mathbf{z},\mathbf{x};\epsilon) \subset \Omega\setminus\Gamma$ for some $\epsilon > 0$. If $\mathbf{y} \in L(\mathbf{z},\mathbf{x};\epsilon)$, then it can be parametrized with $\mathbf{y} = \mathbf{y}(t) \equiv \mathbf{x} + t(\mathbf{z}-\mathbf{x})$ for $-\epsilon \leqslant t \leqslant 1$, $t \neq 0$.

Let us consider two functions defined on $-\epsilon \leqslant t \leqslant 1$, $t \neq 0$ such that $U^+(t) = \frac{1}{2}(1+\frac{|t|}{t})u^+(t)$ and $U^-(t) = \frac{1}{2}(1-\frac{|t|}{t})u^-(t)$ for some functions $u^+(t)$ and $u^-(t)$ satisfying

$$u^+(t)|_{t>0} = u(\mathbf{y}(t)), \quad u^-(t)|_{t<0} = u(\mathbf{y}(t)). \tag{67}$$

Obviously, it holds that $u(\mathbf{y}(t)) = U^+(t) + U^-(t)$ for $-\epsilon \leqslant t \leqslant 1$, $t \neq 0$. Since $u(\mathbf{x}) \in C_B^{m+1}(\Omega \setminus \Gamma)$, Taylor's theorem for $u(\mathbf{y}(t))$ on both sides, $t > 0$ and $t < 0$, enables us to define the functions $u^\pm(t)$ such that, for $-\epsilon \leqslant t \leqslant 1$, $t \neq 0$,

$$u^+(t) = \sum_{k=0}^{m} \frac{1}{k!}\frac{\mathrm{d}^k}{\mathrm{d}t^k} u(\mathbf{y}(t))\bigg|_{t\to 0^+} t^k + R_m(\mathbf{y}(t);\mathbf{x}), \tag{68}$$

$$u^-(t) = \sum_{k=0}^{m} \frac{1}{k!}\frac{\mathrm{d}^k}{\mathrm{d}t^k} u(\mathbf{y}(t))\bigg|_{t\to 0^-} t^k + R_m(\mathbf{y}(t);\mathbf{x}), \tag{69}$$

$$R_m(\mathbf{y}(t);\mathbf{x}) = t^{m+1} \int_0^1 \frac{1}{m!}\frac{\mathrm{d}^{m+1}}{\mathrm{d}t^{m+1}} u(\mathbf{y}(t))\bigg|_{t\to\tau t} (1-\tau)^m \mathrm{d}\tau, \tag{70}$$

where $R_m(\mathbf{y}(t);\mathbf{x})$ is said to be the remainder term. Due to the following derivative formula

$$\frac{d^k}{dt^k} u(\mathbf{x}+t(\mathbf{z}-\mathbf{x})) = \sum_{|\alpha|=k} \frac{k!}{\alpha!} (\mathbf{z}-\mathbf{x})^\alpha (D^\alpha u)(\mathbf{x}+t(\mathbf{z}-\mathbf{x})), \tag{71}$$

if we set $\mathbf{x}^\pm = \mathbf{y}(0^\pm)$, then we have the equivalent expressions for $u^\pm(t)$

$$u^+(t) = \sum_{k=0}^{m} t^k \left(\sum_{|\alpha|=k} \frac{1}{\alpha!} (\mathbf{z}-\mathbf{x})^\alpha (D^\alpha u)(\mathbf{x}^+) \right) + R_m(\mathbf{y}(t);\mathbf{x}), \tag{72}$$

$$u^-(t) = \sum_{k=0}^{m} t^k \left(\sum_{|\alpha|=k} \frac{1}{\alpha!} (\mathbf{z}-\mathbf{x})^\alpha (D^\alpha u)(\mathbf{x}^-) \right) + R_m(\mathbf{y}(t);\mathbf{x}), \tag{73}$$

where the remainder term is expressed as follows:

$$R_m(\mathbf{y}(t);\mathbf{x}) = \sum_{|\alpha|=m+1} \frac{(m+1)!}{\alpha!} (\mathbf{y}(t)-\mathbf{x})^\alpha \int_0^1 \frac{(1-\tau)^m}{m!} (D^\alpha u)(\mathbf{x}+\tau(\mathbf{y}(t)-\mathbf{x}))\,\mathrm{d}\tau. \tag{74}$$

Therefore, we have

$$U^+(t) = \frac{1}{2}\left(1+\frac{|t|}{t}\right)\left(\sum_{|\alpha|\leqslant m} \frac{1}{\alpha!} (\mathbf{y}(t)-\mathbf{x})^\alpha (D^\alpha u)(\mathbf{x}^+) + R_m(\mathbf{y}(t);\mathbf{x}) \right), \tag{75}$$

$$U^-(t) = \frac{1}{2}\left(1-\frac{|t|}{t}\right)\left(\sum_{|\alpha|\leqslant m} \frac{1}{\alpha!} (\mathbf{y}(t)-\mathbf{x})^\alpha (D^\alpha u)(\mathbf{x}^-) + R_m(\mathbf{y}(t);\mathbf{x}) \right), \tag{76}$$

and consequently the following expansion theorem is obtained, for a unit normal vector $\mathbf{n}$ to Γ at $\mathbf{x}$,

$$\begin{aligned} u(\mathbf{y}(t)) &= U^+(t) + U^-(t) \\ &= \sum_{|\alpha|\leqslant m} \frac{\langle D^\alpha u\rangle_{\mathbf{x}}}{\alpha!} (\mathbf{y}(t)-\mathbf{x})^\alpha + \frac{1}{2}\mathrm{sign}(\mathbf{n}\cdot(\mathbf{y}(t)-\mathbf{x})) \sum_{|\alpha|\leqslant m} \frac{[D^\alpha u]_{\mathbf{x}}}{\alpha!} (\mathbf{y}(t)-\mathbf{x})^\alpha + R_m(\mathbf{y}(t);\mathbf{x}) \end{aligned}$$

since the following relation always holds independently of the choice of $\mathbf{n}$:

$$\frac{|t|}{t}(v(\mathbf{x}^+) - v(\mathbf{x}^-)) = \operatorname{sign}(\mathbf{n}\cdot(\mathbf{y}(t)-\mathbf{x}))[v]_{\mathbf{x}} \tag{77}$$

for any discontinuous function v along Γ.

From the remainder term (74), the following estimate holds for any $u(\mathbf{x}) \in C_B^{m+1}(\overline{\Omega \setminus \Gamma})$

$$|R_m(\mathbf{y}(t);\mathbf{x})| \leqslant \left(\sup_{|\alpha|=m+1} \|D^\alpha u(\mathbf{x})\|_{C^0(\Omega\setminus\Gamma)} \sum_{|\alpha|=m+1} \frac{1}{\alpha!}\right)|\mathbf{y}(t)-\mathbf{x}|^{m+1}.$$

We are done with the proof. □

Appendix B. Derivation of extrinsic meshfree approximation formula

In the moving least square meshfree approximation method[10], the coefficient vector $\mathbf{a}(\bar{\mathbf{x}})$ that appears in the local meshfree approximation (21) is calculated by minimizing the functional (22). After some algebraic manipulations, we have the following local approximation near $\bar{\mathbf{x}}$:

$$u_{\bar{\mathbf{x}}}(\mathbf{x}) = \frac{1}{2}\left[\frac{\partial u}{\partial n}\right]_{\bar{\mathbf{x}}_\Gamma} \chi_{\Omega^s}(\bar{\mathbf{x}}) b_\Gamma(\mathbf{x},\bar{\mathbf{x}}) + \sum_{\mathbf{x}_I\in\Lambda}\left[\mathbf{P}_m\left(\frac{\mathbf{x}-\bar{\mathbf{x}}}{\rho_{\bar{\mathbf{x}}}}\right)\cdot M(\bar{\mathbf{x}})^{-1}\mathbf{P}_m\left(\frac{\mathbf{x}_I-\bar{\mathbf{x}}}{\rho_{\bar{\mathbf{x}}}}\right)W_{\bar{\mathbf{x}}}(\mathbf{x}_I)\right]u^*(\mathbf{x}_I,\bar{\mathbf{x}}), \tag{78}$$

where the function u^* is defined by

$$u^*(\mathbf{x}_I,\bar{\mathbf{x}}) \equiv u(\mathbf{x}_I) - \frac{1}{2}\left[\frac{\partial u}{\partial n}\right]_{\bar{\mathbf{x}}_\Gamma} \chi_{\Omega^s}(\bar{\mathbf{x}}) b_\Gamma(\mathbf{x}_I,\bar{\mathbf{x}}). \tag{79}$$

and $M(\bar{\mathbf{x}})$ is the moment matrix defined as

$$M(\bar{\mathbf{x}}) \equiv \sum_{\mathbf{x}_I\in\Lambda}\mathbf{P}_m\left(\frac{\mathbf{x}_I-\bar{\mathbf{x}}}{\rho_{\bar{\mathbf{x}}}}\right)\mathbf{P}_m^{\mathrm{T}}\left(\frac{\mathbf{x}_I-\bar{\mathbf{x}}}{\rho_{\bar{\mathbf{x}}}}\right)W_{\bar{\mathbf{x}}}(\mathbf{x}_I). \tag{80}$$

Since a good approximation takes place at the center point $\bar{\mathbf{x}}$ if the radial window function W decays rapidly away from the center $\bar{\mathbf{x}}$, we can infer that the following diffuse derivative approximations make sense:

$$\mathscr{D}_h^\beta u(\mathbf{x}) \equiv \lim_{\bar{\mathbf{x}}\to\mathbf{x}} D_{\mathbf{x}}^\beta u_{\bar{\mathbf{x}}}(\mathbf{x}), \quad |\beta| \leqslant m. \tag{81}$$

Following up the procedure (81), we can obtain

$$\mathscr{D}_h^\beta u(\mathbf{x}) = \frac{1}{2}\left[\frac{\partial u}{\partial n}\right]_{\mathbf{x}_\Gamma} \chi_{\Omega^s}(\mathbf{x}) D_{\mathbf{x}}^\beta b_\Gamma(\mathbf{x},\bar{\mathbf{x}})\big|_{\bar{\mathbf{x}}=\mathbf{x}} + \sum_{\mathbf{x}_I\in\Lambda}\psi_I^{[\beta]}(\mathbf{x})\left(u(\mathbf{x}_I) - \frac{1}{2}\left[\frac{\partial u}{\partial n}\right]_{\mathbf{x}_\Gamma}\chi_{\Omega^s}(\mathbf{x}) b_\Gamma(\mathbf{x}_I,\mathbf{x})\right), \tag{82}$$

where $\psi_I^{[\beta]}(\mathbf{x})$ are the shape functions written as

$$\psi_I^{[\beta]}(\mathbf{x}) = \frac{1}{\rho_{\mathbf{x}}^{|\beta|}} D_{\mathbf{x}}^\beta \mathbf{P}_m(0)\cdot M(\mathbf{x})^{-1}\mathbf{P}_m\left(\frac{\mathbf{x}_I-\mathbf{x}}{\rho_{\mathbf{x}}}\right)W_{\mathbf{x}}(\mathbf{x}_I). \tag{83}$$

After collecting terms involving the local wedge function b_Γ, our extrinsic meshfree approximation can be achieved. It is important that the shape functions $\psi_I^{[\beta]}(\mathbf{x})$'s in (82) are identical to the regular shape functions derived from the polynomial basis only. Furthermore, if we assume the boundedness of the norm of inverse moment matrix, then we obtain the following estimate

$$|\psi_I^{[\beta]}(\mathbf{x})| \leqslant C\frac{1}{\rho_{\mathbf{x}}^{|\beta|}}. \tag{84}$$

Appendix C. Proof of the reproducing of the normal derivative jump across the interface

Assume $u(\mathbf{x}) \in C_B^{m+1}(\Omega \setminus \Gamma) \cap C^0(\overline{\Omega})$. Let $\mathbf{n}$ be a prescribed normal vector to the interface Γ at $\mathbf{x}^* \in \Gamma$ and $\mathbf{x}^{\pm}$ be the limit points on either side of Γ, i.e., $\mathbf{x}^{\pm} = \lim_{t \to 0^{\pm}} \mathbf{x}^* + t\mathbf{n}$. We claim that for any $\mathbf{x}^* \in \Gamma$

$$\nabla^h u \cdot \mathbf{n}|_{\mathbf{x}^+} - \nabla^h u \cdot \mathbf{n}|_{\mathbf{x}^-} = \left[\frac{\partial u}{\partial n}\right]_{\mathbf{x}_\Gamma^*}, \tag{85}$$

where ∇^h is the extrinsic meshfree gradient operator defined by

$$\nabla^h u = (\mathscr{D}_h^{(1,0,\ldots,0)} u, \ldots, \mathscr{D}_h^{(0,\ldots,0,1)} u). \tag{86}$$

Since the coefficient function $\left[\frac{\partial u}{\partial n}\right]_{\mathbf{x}_\Gamma}$ has the same value at both $\mathbf{x}^+$ and $\mathbf{x}^-$, i.e.,

$$\left[\frac{\partial u}{\partial n}\right]_{\mathbf{x}_\Gamma^+} = \left[\frac{\partial u}{\partial n}\right]_{\mathbf{x}_\Gamma^-} = \left[\frac{\partial u}{\partial n}\right]_{\mathbf{x}_\Gamma^*}, \tag{87}$$

we have

$$\begin{aligned} \nabla^h u \cdot \mathbf{n}|_{\mathbf{x}^+} - \nabla^h u \cdot \mathbf{n}|_{\mathbf{x}^-} &= \left(\nabla^h u|_{\mathbf{x}^+} - \nabla^h u|_{\mathbf{x}^-}\right) \cdot \mathbf{n} \\ &= \frac{1}{2}\left[\frac{\partial u}{\partial n}\right]_{\mathbf{x}_\Gamma^*} \left(\nabla^h S_\Gamma(\mathbf{x}^+) - \nabla^h S_\Gamma(\mathbf{x}^-)\right) \cdot \mathbf{n} + \sum_{\mathbf{x}_I \in \Lambda} u(\mathbf{x}_I)\left(\nabla^h \psi_I(\mathbf{x}^+) - \nabla^h \psi_I(\mathbf{x}^-)\right) \cdot \mathbf{n}, \end{aligned} \tag{88}$$

where the terms $\nabla^h S_\Gamma$ and $\nabla\, {}^h\psi_I$ are defined as

$$\nabla^h S_\Gamma \equiv (S_\Gamma^{[(1,0,\ldots,0)]}, \ldots, S_\Gamma^{[(0,\ldots,0,1)]}), \tag{89}$$

$$\nabla^h \psi_I \equiv (\psi_I^{[(1,0,\ldots,0)]}, \ldots, \psi_I^{[(0,\ldots,0,1)]}). \tag{90}$$

From the continuity on the interface of the shape functions $\psi_I^{[\beta]}$'s for any $\mathbf{x}_I \in \Lambda$ and β with $|\beta| \leqslant m$, the last term in (88) vanishes. Thus, the extrinsic meshfree approximation (24), together with the definition of singular shape functions (25) and the derivative formula (19) for the local wedge function, leads the following:

$$\nabla^h u \cdot \mathbf{n}|_{\mathbf{x}^+} - \nabla^h u \cdot \mathbf{n}|_{\mathbf{x}^-} = \frac{1}{2}\left[\frac{\partial u}{\partial n}\right]_{\mathbf{x}_\Gamma^*} (\mathbf{n}_\Gamma(\mathbf{x}^+) - \mathbf{n}_\Gamma(\mathbf{x}^-)) \cdot \mathbf{n} \tag{91}$$

since the function $b_\Gamma(\mathbf{x}_I, \mathbf{x})$ is continuous on Γ in the variable $\mathbf{x}$ for any $\mathbf{x}_I \in \Lambda$ and hence

$$\sum_{\mathbf{x}_I \in \Lambda} u(\mathbf{x}_I)\left(b_\Gamma(\mathbf{x}_I, \mathbf{x}^+)\nabla^h \psi_I(\mathbf{x}^+) - b_\Gamma(\mathbf{x}_I, \mathbf{x}^-)\nabla^h \psi_I(\mathbf{x}^-)\right) \cdot \mathbf{n} = 0. \tag{92}$$

From the definition of the map $\mathbf{n}_\Gamma$, we have

$$\mathbf{n}_\Gamma(\mathbf{x}^+) = \mathbf{n} = -\mathbf{n}_\Gamma(\mathbf{x}^-). \tag{93}$$

Therefore, (91) is rewritten as follows:

$$\nabla^h u \cdot \mathbf{n}|_{\mathbf{x}^+} - \nabla^h u \cdot \mathbf{n}|_{\mathbf{x}^-} = \left[\frac{\partial u}{\partial n}\right]_{\mathbf{x}_\Gamma^*}, \tag{94}$$

which proves the Eq. (28).

References

[1] I. Babuška, The finite element method for elliptic equations with discontinuous coefficients, Computing 5 (1970) 207–213.
[2] T. Belytschko, N. Moës, S. Usui, N. Sukumar, C. Parimi, Arbitrary discontinuities in finite elements, Int. J. Numer. Meth. Engng. 50 (2001) 993–1013.
[3] P.A. Berthelsen, A decomposed immersed interface method for variable coefficient elliptic equations with non-smooth and discontinuous solutions, J. Comput. Phys. 197 (2004) 364–386.

[4] J. Chessa, H. Wang, T. Belytschko, On the construction of blending elements for local partition of unity enriched finite elements, Int. J. Numer. Meth. Engng. 57 (2003) 1015–1038.
[5] R.P. Fedkiw, T. Aslam, B. Merriman, S. Osher, A non-oscillatory Eulerian approach to interfaces in multimaterial flows (The Ghost Fluid Method), J. Comput. Phys. 152 (1999) 457–492.
[6] F. Gibou, R.P. Fedkiw, L.-T. Cheng, M. Kang, Second order accurate symmetric discretization of the Poisson equation on irregular domains, J. Comput. Phys. 176 (2002) 205–227.
[7] W. Han, X. Meng, Error analysis of the reproducing kernel particle method, Comput. Methods Appl. Mech. Engrg. 190 (2001) 6157–6181.
[8] S. Hou, X.-D. Liu, A numerical method for solving variable coefficient elliptic equation with interfaces, J. Comput. Phys. 202 (2005) 411–445.
[9] D.W. Kim, H.-K. Kim, Point collocation method based on the FMLSRK approximation for electromagnetic field analysis, IEEE Trans. Magn. 40 (2) (2004) 1029–1032.
[10] D.W. Kim, W.K. Liu, Maximum principle and convergence analysis for the meshfree point collocation method, SIAM J. Numer. Anal. 44 (2) (2006) 515–539.
[11] D.W. Kim, Y. Kim, Point collocation methods using the fast moving least-square reproducing kernel approximation, Int. J. Numer. Meth. Engng. 56 (2003) 1445–1464.
[12] Y. Krongauz, T. Belytschko, EFG Approximation with discontinuous derivatives, Int. J. Numer. Meth. Engng. 41 (1998) 1215–1233.
[13] R.J. LeVeque, Z. Li, The immersed interface method for elliptic equations with discontinuous coefficients and singular sources, SIAM J. Numer. Anal. 31 (1994) 1019–1044.
[14] Z. Li, A fast iterative algorithm for elliptic interface problems, SIAM J. Numer. Anal. 35 (1) (1998) 230–254.
[15] S. Li, W.K. Liu, Meshfree Particle Methods, Springer, Berlin Heidelberg New York, 2004.
[16] W.K. Liu, S. Jun, Y.F. Zhang, Reproducing Kernel Particle Methods, Int. J. Numer. Meth. Fluids 20 (1995) 1081–1106.
[17] W.K. Liu, S. Jun, S. Li, J. Adee, T. Belytschko, Reproducing Kernel Particle Methods for Structural Dynamics, Int. J. Numer. Meth. Engng. 38 (1995) 1655–1679.
[18] W.K. Liu, S. Li, T. Belytschko, Moving least square reproducing kernel methods (I) methodology and convergence, Comput. Methods Appl. Mech. Engrg. 143 (1996) 422–433.
[19] X.-D. Liu, R.P. Fedkiw, M. Kang, A boundary condition capturing method for Poisson's equation on irregular domains, J. Comput. Phys. 160 (2000) 151–178.
[20] X.-D. Liu, T.C. Sideris, Convergence of the ghost fluid method for elliptic equations with interfaces, Math. Comp. 72 (2003) 1731–1746.
[21] Y. Liu, L. Zhang, X. Wang, W.K. Liu, Coupling of Navier–Stokes equations with protein molecular dynamics and its application to Hemodynamics, Int. J. Numer. Meth. Fluids 46 (12) (2004) 1237–1252.
[22] H. Lu, D.W. Kim, W.K. Liu, Treatment of discontinuity in the reproducing kernel element method, Int. J. Numer. Meth. Engng. 63 (2005) 241–255.
[23] R.J. Mackinnon, G.F. Carey, Treatment of material discontinuities in finite element computations, Int. J. Numer. Meth. Engng. 24 (1987) 393–417.
[24] N. Moës, J. Dolbow, T. Belytschko, A finite element method for crack growth without remeshing, Int. J. Numer. Meth. Engng. 46 (1) (1999) 131–150.
[25] C.S. Peskin, The immersed boundary method, Acta Numer. 11 (2002) 479–517.
[26] A. Wiegmann, K.P. Bube, The explicit-jump immersed interface method: Finite difference methods for PDEs with piecewise smooth solutions, SIAM J. Numer. Anal. 37 (3) (2000) 827–862.
[27] L. Zhang, A. Gerstenberger, X. Wang, W.K. Liu, Immersed finite element method, Comput. Methods Appl. Mech. Engrg. 193 (2004) 2051–2067.